LBL-14761
Preprint c.2

Lawrence Berkeley Laboratory

UNIVERSITY OF CALIFORNIA

RECEIVED
LAWRENCE
BERKELEY LABORATORY
SEP 30 1982
LIBRARY AND
DOCUMENTS SECTION

Materials & Molecular Research Division

Submitted to the Journal of the Electro Analytical Chemical Society

LEED ANALYSIS OF ELECTRODE SURFACES: STRUCTURAL EFFECTS OF POTENTIODYNAMIC CYCLING ON Pt SINGLE CRYSTALS

F.T. Wagner and P.N. Ross, Jr.

July 1982

TWO-WEEK LOAN COPY

This is a Library Circulating Copy which may be borrowed for two weeks. For a personal retention copy, call Tech. Info. Division, Ext. 6782

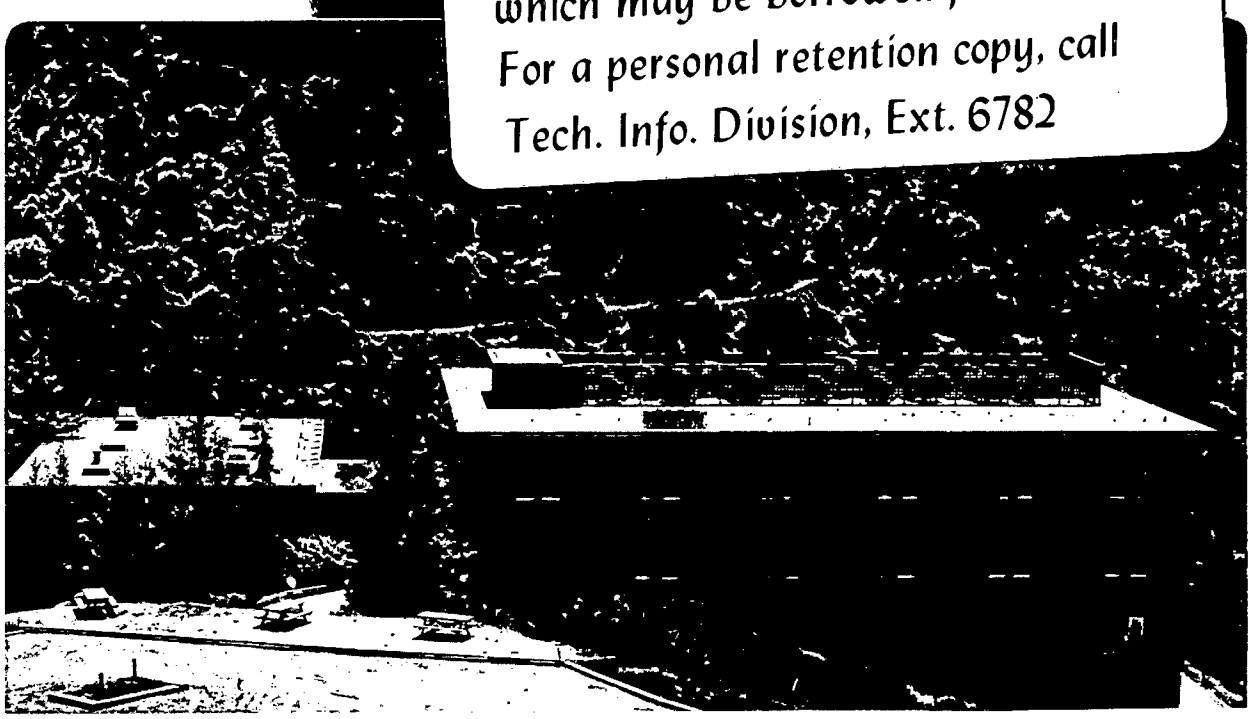

LBL-14761 c.2

Prepared for the U.S. Department of Energy under Contract DE-AC03-76SF00098

DISCLAIMER

This document was prepared as an account of work sponsored by the United States Government. While this document is believed to contain correct information, neither the United States Government nor any agency thereof, nor the Regents of the University of California, nor any of their employees, makes any warranty, express or implied, or assumes any legal responsibility for the accuracy, completeness, or usefulness of any information, apparatus, product, or process disclosed, or represents that its use would not infringe privately owned rights. Reference herein to any specific commercial product, process, or service by its trade name, trademark, manufacturer, or otherwise, does not necessarily constitute or imply its endorsement, recommendation, or favoring by the United States Government or any agency thereof, or the Regents of the University of California. The views and opinions of authors expressed herein do not necessarily state or reflect those of the United States Government or any agency thereof or the Regents of the University of California.

LEED ANALYSIS OF ELECTRODE SURFACES:
STRUCTURAL EFFECTS OF POTENTIODYNAMIC CYCLING ON Pt SINGLE CRYSTALS

F. T. Wagner and P. N. Ross, Jr.

Materials and Molecular Research Division
Lawrence Berkeley Laboratory
University of California
Berkeley, CA 94720

ABSTRACT

An ultra-high vacuum Low Energy Electron Diffraction apparatus directly coupled to a three-electrode electrochemical cell was used to identify the atomic-scale structural changes induced by potentiodynamic cycling of a well-characterized Pt (100) surface in 0.3 M aqueous HF. Cycling between the hydrogen electrosorption region and the edge of the oxygen electrosorption region (0 - 0.82 V RHE) caused no discernable change in the Pt (100)-1 x 1 LEED pattern. However, cycling well into the oxygen electrosorption region (to 1.58 V RHE) produced LEED patterns characterized by alternate broadened and sharp spots. The breadth of a given spot fluctuated with the energy of the incident electron beam in a manner consistent with the formation of random monatomic-height steps on the surface. From the maximum spot width a mean terrace width of 5-7 atoms was estimated. Cyclic voltammetry (0 - 0.8V) on vacuum-prepared Pt (100) and (111) surfaces showed features not seen on "single-crystal" surfaces cleaned by potentiodynamic cycling into the oxygen electrosorption region. Pt (100) showed excess cathodic charge in the "hydrogen electrosorption" region, a cathodic spike during the anodic sweep just above the hydrogen region, and an associated, highly irreversible, couple in the region 0.4 - 0.8 V RHE. Intentional adsorption of CO accentuated these features. Pt (111) showed

no cathodic spike and a highly reversible couple at 0.76 V. Sweeping up to oxygen evolution potentials removed the "anomalous" peaks on both surfaces, yielding single hydrogen electrosorption peaks in agreement with previous work. The present work suggests that the anomalous peaks are due to structure-sensitive reactions with impurities which are irreversibly oxidized during potential excursions into the oxygen electrosorption region.

(1) INTRODUCTION

It is of both technological and fundamental importance to develop an understanding of the changes in the morphology of electrode surfaces when subject to various electrochemical treatments. In battery systems, metal electrodes are cycled either between oxide states, between the metallic and the oxide states, or between a solvated state and the metallic state. To understand what happens in such systems at the atomic level requires a method of following the changes in the atomic structure of the electrode surface. Low Energy Electron Diffraction (LEED) is now a well-developed and still improving method for surface structure determination that is used in virtually every contemporary study of surfaces in vacuum. It should be possible, under certain conditions, to make definitive structure determination by LEED analysis of electrode surfaces ex situ, thereby considerably advancing the state of understanding the transformations occurring at electrode surfaces.

In this report, we review the LEED theory with regard to the determination of the structure of nearly-ordered surfaces containing characteristic imperfections and show how the LEED apparatus can be interfaced to an electrochemical cell. The electrode system studied here is the Pt electrode in dilute HF electrolyte, and in particular the effects

of potentiodynamic cycling on the structure of the low index single crystal surfaces. Some previous studies of Pt single crystal electrodes have shown hydrogen electrosorption behavior directly related to the behavior of polycrystalline electrodes (1-4), while others (5,6) claim that more complex behavior is observed if the surfaces are not cycled through the Pt oxide formation/reduction potential region. The results reported here confirm that complex behavior is observed on (111) and (100) surfaces not cycled through oxide formation/reduction, and that the simpler behavior is also observed after limited cycling to oxygen evolution potential (1.5-1.6 V RHE). A LEED analysis of the (100) surface is presented here that indicates this limited cycling alters the long-range ordering (>100 Å) of the surface but local ordering (13-19 Å) is preserved. It is concluded that the distinction between the two kinds of behavior is not caused by a structural transformation of the surface, but by other phenomena, e. g. the oxidation of impurities.

(2) LEED AND THE STUDY OF SURFACE DEFECTS

Low energy electron diffraction (LEED) provides a sensitive probe of the atomic-scale structure of solid surfaces. Although early LEED theory [7] was restricted to the treatment of perfect low index surfaces or surfaces with perfectly ordered arrays of steps [8,9], the technique has been advanced to deal also with statistical distribution of steps [10,11], and other forms of surface defects [12,13,14]. Improvements in both theory and experimental technique are now allowing the type, size distribution, and density of imperfections to be identified.

The strong interactions between slow electrons and atoms which lend LEED its high surface sensitivity also make its theory more complex than

that for x-ray diffraction. Complete theoretical description of low energy electron scattering of sufficient precision for quantitative determination of atomic positions within the surface unit cell requires complex treatments of the variation of diffracted beam intensity with kinetic energy, taking into account multiple scattering events. However, the location, width, and/or splitting of diffracted beams can, for the most part, be accounted for with kinematic (single-scattering) theory closely analogous to that for x-ray diffraction. The beam energy-dependent effects of different classes of surface defects can be most easily visualized by combining elements of kinematic theory with a geometric representation of coherent elastic scattering, the Ewald construction.

Figure 1 shows a cross-section of the Ewald construction (taken along one of the principle symmetry axes of the surface) for normal-incidence LEED. Whereas a three-dimensional (3-D) real-space lattice transforms into reciprocal (momentum) space as a 3-D lattice of points, a two-dimensional (2-D) real-space mesh transforms into an array of rods normal to the surface and evenly spaced at $2\pi/a$, where a is the real-space periodicity in the direction of interest. The incident wavevector $\vec{k}_o$ ($|\vec{k}_o| = 2\pi/\lambda = 0.513U^{1/2}$ where λ is the electron wavelength in Å and U is the incident electron energy in eV) is drawn to end at the reciprocal space origin, making an angle to the lattice rods equal to the angle of incidence (here 0°). The assumption of elastic scattering ($|\vec{k}| = |\vec{k}_o|$ with $\vec{k}$ the scattered wavevector) is shown graphically by drawing a sphere of radius $|\vec{k}_o|$. Coherent scattering from a perfect infinite 2-D mesh occurs only when the tangential momentum transfer equals a surface reciprocal lattice vector:

$$S_{||} = k_{||} - k_{o_{||}} = \vec{G}_{h_1,h_2} \qquad (1)$$

This condition is satisfied graphically when the tip of $\vec{k}$ lies on a reciprocal lattice rod. Simultaneously coherent and elastic scattering occurs when $\vec{k}$ lies at the intersection of a lattice rod and the Ewald sphere. The angular position of the resulting LEED beam is given by θ, the angle between $\vec{k}$ and the rods.

The 2-D Ewald construction is strictly valid only for an ideal infinite 2-D mesh of point scatterers. In fact, LEED shows some sensitivity to the third dimension; the importance of the 3-D lattice point ordered in the analysis of imperfect surfaces will be shown shortly. Smaller domain sizes below the instrumental coherence length (typically 100-300 Å in commercial instruments [13], but up to 10,000 Å or more for advanced equipment [15,16]) cause a measurable broadening of all of the LEED beams at all incident energies. Thermal vibration of atoms about their equilibrium position decreases beam intensity without affecting sharpness and leads to a general diffuse background (Debye-Waller effect). Inelastically scattered electrons, which are incompletely filtered out by LEED optics, would produce a diffuse background even from a perfect lattice at zero degrees Kelvin. Point defects such as random adatoms, vacancies in the substrate surface or a disordered overlayer would also add a diffuse background to the diffraction pattern of the substrate. This diversity of background sources complicates quantitative analysis of background intensity. Jona [17] has shown that addition of ~20% of a monolayer of random Si atoms to an ordered Si surface causes no obvious

change in the diffraction pattern.

Surface defects can introduce new periodicities with dimensions close enough to the incident electron wavelength to produce new spots or changes in spot shapes. The diffraction effects of periodic steps along the (010) and (011) directions of a fcc (100) crystal surface are shown in the Ewald constructions of Fig. 2. Lattice rods are drawn in for both the atomic periodicity within a terrace (medium lines) and the step periodicity (light lines). The diffraction conditions for both periodicities are satisfied at the intersections of the lattice rods (filled circles); when the Ewald circle passes through such an intersection a single diffraction spot is seen (e.g. the (11) spot at 175 eV). If the steps have monoatomic heights, as shown in Fig. 2, the intersections are also the reciprocal lattice points of the 3-D crystal and signify coherent scattering from adjacent layers parallel to the surface. Because of the limited number of scatterers within each terrace, the interference factor for the terrace will show considerable angular width. At $\vec{k}$ values away from the rod intersections, diffraction intensity is governed by the product of the broad terrace interference function with the sharp step interference function, and split spots result. Midway in k-space between rod intersections, two step rods evenly straddle the broadened terrace rod (open circles in Fig. 2), and a symmetrically split pair of spots of equal intensity will be observed, (e.g. (10) beam at 175 eV). The angular splitting of the pair is inversely related to the terrace width ℓ. If the steps were of diatomic rather than monatomic height, the angle between the two sets of lattice rods would double, the reciprocal space distances between rod intersections would halve, and single unsplit diffraction

beams would be observed at more closely spaced incident beam energies. Given diffraction data from a stepped surface, one can determine the terrace width from the angular splitting of the spots and the step height from the incident energies at which the beams are not split [9].

Using an average pair correlation function, Houston and Park [10] have shown that resolvable split beams are to be expected even for surfaces with a distribution of terrace widths. When the terrace widths become sufficiently random, however, resolution of the split spots is lost and diffracted intensity appears as single spots with widths modulated by changes in incident energy. The Ewald construction for a surface with up and down monatomic steps and random terrace widths is shown in Fig. 3. Lu, et al. [11] have developed closed-form solutions relating LEED spot angular profile to mean terrace width for a number of step height and terrace width distributions. If only diatomic step heights are present, the spot width variation with beam energy will have a periodicity half shown in Fig. 3. A distribution of small (<5 atom) step heights leads to global minima in spot widths at the energies expected for monatomic steps with local minima in width of higher periodicity. If large step sizes predominate in a broad distribution, the intermediate minima become much smaller than the global minima which in turn become very sharp.

While step-like imperfections, either periodic or random, lead to distinctive spot size vs. beam energy behavior, other types of surface imperfections yield less dramatic effects on diffraction patterns which nonetheless can be analyzed in some detail, as done by Henzler [13] and Lagally [14]. Beam broadenings due to finite domain size and diffuse background from point defects have already been discussed above. Random strain at the surface preferentially broadens diffraction spots of higher order, leaving the (0 0) spot sharp. A metallic "single crystal" actually consists of a mosaic of crystallites with diameters on the order of 1μm and misorientations on the order of 0.1°. Over these distances intensities, not amplitudes, are added, and the LEED pattern is a sum of patterns from each crystallite with the angular divergence between crystallites causing increased apparent broadening of all spots as the beam energy is increased. A partial overlayer may consist of domains which are commensurate with the substrate, but which are out of phase with one another. If these "anti-phase domains" are smaller than the instrumental electron coherence length, a LEED pattern containing both sharp and broadened (or split) spots may result. In this case, the relative widths of any two spots of different symmetry remain unchanged by a variation in the incident beam energy. This invariance allows ready distinction between LEED patterns due to anti-phase domains and those due to steps. Under some conditions generally involving chemical etching or thermal annealing, a given crystal face may facet into microfaces of more stable orientations. If the facets are larger than the coherence length of the instrument, two (or more) independent LEED patterns will be seen simultaneously. Each pattern will have its own (0 0) spot towards which the other spots will migrate as

the beam energy is increased. Since all facets are part of the same 3-D crystal, spots due to the different faces will coalesce at beam energies corresponding to 3-D reciprocal lattice points to form a single sharp spot. If the beam energy is then increased, the spot splits, with the diffraction spot due to each facet orientation moving off towards the appropriate (0 0) beam. As the facet size drops below the instrumental coherence length, resolution of the split spots is lost and one obtains instead a single spot broadened out towards the various (0 0) beams. At the limit of very small facet sizes, the LEED pattern would be indistinguishable from that for a randomly stepped surface. In this limit, however, the real-space surface would also be aptly described by either the faceted or the stepped surface model.

LEED has the potential to identify a number of types of defects on a crystalline surface and, under favorable conditions, can give quantitative information on the density and size distributions of such defects. An absolute image of the real-space surface cannot be obtained by the LEED technique since intensities, not amplitudes, are detected and phase information is lost. But, as will be shown in this paper, the information derived from LEED is sufficient to provide better understanding of structural changes incurred in metals when the surface is sequentially oxidized and reduced electrochemically.

(3) EXPERIMENTAL

(3.1) Electrode, mount, and manipulators

Pt (100) and (111) disks were cut, oriented, and polished by standard techniques, cleaned in hydrofluoric and fuming nitric acids, and gold-brazed onto thin Ta holders leaving gold fillets which masked most of the crystal edges. The crystal mount was held in a stainless steel frame which allowed both emplacement onto the UHV manipulator (equipped for radiative heating of the sample holder) and withdrawal to the electrochemical cell via a long-throw magnetically coupled manipulator (C-1 in Fig. 4). A second magnetically-coupled manipulator (C-2 in Fig. 4) lowered the electrochemical cell past its isolation gate valve to the level of the crystal.

(3.2) Surface Analytical Chamber

Surface preparation and analysis were performed in the bakeable ion-pumped UHV chamber shown on the right of Fig. 4. Base and working pressures of 5×10^{-11} and 4×10^{-10} torr, respectively, were standard. A Varian 4-grid LEED apparatus with off-axis cathode was mounted opposite the 8" viewport through which LEED patterns could be recorded with a Polaroid CU-5 camera. Auger electron spectroscopy was performed with a Varian (Model 981-2707) high-resolution cylindrical mirror analyzer with 10 keV integral electron gun. The electron beam could be rastered to obtain an absorbed current and/or secondary electron image of the crystal permitting precise choice of the analysis area. A Spectramass 1000 quadrupole mass analyzer mounted either on the UHV or transfer chamber was used for identification of background gas components and for thermal desorption spectroscopy. Electrodes were cleaned by argon ion sputtering followed by annealing at 1100 K *in vacuo*, at times with a preceeding 900K

anneal in 3 x 10^{-8} torr O_2. A separate variable leak valve allowed for dosing of the crystal with other gases.

(3.3) Transfer Chamber

The transfer chamber (B in Fig. 4) was pumped to 2 x 10^{-9} torr with a liquid nitrogen-trapped 110 l/s Balzers turbomolecular pump and was baked out at 150°C prior to experiments. After the cleaned and characterized crystal has been introduced from the analysis chamber, the turbopump is isolated, and the transfer chamber is backfilled to nearly atmospheric pressure with argon, (Matheson grade, 99.9995% quoted purity), and the previously prepared electrochemical cell is lowered.

(3.4) Electrochemical Apparatus

The internal electrochemical cell consists of a 0.63 cm O.D. Pt ring-Pd disk assembly press-fit into a polytetrafluoroethylene (PTFE) plate; the ring and disk serve as counter and reference electrodes, respectively. Contact with the single-crystal working electrode is made through an insulated Pt foil spring. After a gate-valve to the transfer chamber is closed, the cell compartment is backfilled with Ar. A droplet (10-100μℓ) of the 0.3 M aqueous HF electrolyte (prepared from Baker Ultrex 48% HF and Harleco water) is introduced to the cell from an external PTFE reservoir (D in Fig. 4) through a halopolymer needle valve and PTFE capillary. The Pd disk is electrolytically charged with hydrogen against a movable Pt wire probe electrode and holds a potential of +0.08V vs. RHE (the reversible hydrogen electrode in the same electrolyte, to which all potentials in this paper will refer) for a time period sufficient to complete the experiments of interest here. After the cell is flushed twice with fresh electrolyte to remove free oxygen and hydrogen, it is lowered to

allow contact with the single crystal electrode under potentiostatic control.

Linear sweep cyclic voltammetry, usually at 100 mV/S, is performed with a PAR model 173 potentiostat equipped with a model 179 digital coulometer and driven by a programmable sweep generator built in-house. At the conclusion of cyclic voltammetry the crystal is held at 0.4 V, the transfer chamber is slightly overpressurized with Ar, and the electrolyte is driven out the PTFE capillary. This procedure gives a clean separation of electrolyte from the crystal and probably leaves an electrolyte film thinner than 40Å on the surface [18]. The transfer chamber is then evacuated and the sample returned to the analysis chamber.

The contact area between the crystal and the electrolyte was determined by electron imaging performed in the surface analytical chamber. Contact areas in this work range from 0.2 to 0.7 cm^2. Charge passed per surface Pt atom was calculated using the measured contact area and the ideal surface capacities corresponding to one electron per surface Pt atom of 209$\mu C/cm^2$ for Pt (100)-1 x 1 and 240$\mu C/cm^2$ for Pt (111).

(4) RESULTS

(4.1) LEED and AES of Potentiodynamically Cycled Pt (100)

Figure 5 shows the LEED pattern for a clean Pt (100) surface prepared in UHV. The complex pattern of multiple spots (the "5 x 20" reconstruction) is generally believed to result from the presence of a hexagonally closest packed surface layer on top of the square meshed substrate [19]. In the presence of small coverages of almost any adsorbate this reconstructed surface reverts back to the 1 x 1 termination of the bulk structure [20]. This

transition entails a decrease of at most ~15% in the number of surface platinum atoms per unit area. In our apparatus the 5 x 20 reconstruction survives at least 15 minutes in the unpumped transfer chamber as long as no argon is admitted. However, after a backfill to atmospheric pressure followed by pumpdown, the surface transforms to the 1 x 1 structure as shown by the LEED pattern in Fig. 6a. All of the 1 x 1 spots are sharp at all energies, but an increased diffuse background is apparent. The source of the diffuse background is made evident by Fig. 7, which shows Auger spectra at various stages in the transfer process (spectra c and d are from the same surfaces which yielded the LEED patterns in Fig. 6a and b, respectively). After an argon backfill the crystal shows a carbon Auger peak at 272 eV corresponding to a C/Pt surface atomic ratio of 0.9 as per the in situ radiotracer calibration of the Auger peak height ratio by Davis, et al. [21]. A single graphite basal plane corresponds to C/Pt=4.7. The Cl peaks at 181 eV, though appearing rather large in Figs. 6c and d, correspond to a maximum Cl/Pt atomic ratio of less than 0.05 based on either a calibration from the work of Davis [22] or an Auger spectra for HCl on Pt published by Garwood and Hubbard [23]. The persistence of the C Auger signal after heating to ~1200K allows the exclusion of a number of possible impurities in the argon as the major source of the Auger-detectable carbon, e.g. CO, CO_2, oxygenated C_1 and C_2 compounds, and small ($<C_6$) alkanes. However, olefins as small as ethylene give the observed irreversible adsorption on Pt surfaces [24]. On Pt (100) ethylene gives a disordered or highly diffuse LEED pattern even from pure vapor unless

adsorbed at high (10^{-1} torr) partial pressures [25,26]. It thus seems reasonable to ascribe the diffuse background in Fig. 5 to a disordered carbonaceous (possibly olefinic) overlayer derived from impurities in the backfill gas. Although CO cannot be the major source of Auger-detectable carbon, it may be present on the surface. Electron beam-induced desorption and decomposition of CO on transition metal surfaces [27] prevent accurate quantitation of CO by AES. Additional purification of the commercial high-purity gas and detailed analysis of surface contaminants by multiplexed thermal desorption spectroscopy will be carried out in future experiments.

Figures 6b and 7d show the LEED pattern and Auger spectrum for a UHV-prepared Pt (100) surface which was contacted with 0.3 MHF at 0.4 V RHE, swept ten times at 100 mV/s between 0.02 and 0.82 V RHE, and separated from the electrolyte while potentiostated at 0.4 V. No significant differences between this LEED pattern and the one exposed merely to the Ar backfill (Fig. 6a) are observed by LEED at any incident beam energy. Thus contact with the electrolyte and potentiodynamic cycling to the edge of the oxygen electrosorption region causes no discernable change in the structure of the surface. The Auger spectrum shows only slight increases in the C and Cl impurities. The lack of an Auger signal due to surface fluoride (650 eV), even in spectra of higher sensitivity, indicates that the electrolyte does, in fact, volatilize cleanly.

Figures 8a, b, and c show the effects of extending the upper sweep limit to 1.58 V RHE on LEED patterns taken at various incident beam energies. At 178 eV the (11) spots are sharp while the (10) and (20) spots are broadened. At 134 eV the (10) and (20) spots are sharp while the (11)

spots are broadened. At 114 eV the (11) spots are sharp, the (10) spots are broadened and the (20) spots are off the screen. The alternating pattern continues down to the lowest beam energy at which spots are visible, about 50 eV. The effect, though somewhat obscured by the diffuse background from the disordered carbon contaminant, has been shown to be highly reproducible on two different Pt (100) crystals.

Of all the defect types discussed in section (2), only random steps can yield LEED patterns consistent with the observed periodic variation in the angular width of diffraction spots as the incident electron energy is changed. The fact that every LEED beam is sharp at some energies indicates that most surface Pt atoms are still in lattice positions of the 3-D crystal. These LEED patterns indicate that limited potentiodynamic cycling into the "oxide region" has shifted many atoms out of the ideal planar surface but has left them in 3-D lattice sites. The energies at which sharp (10), (20), and (11) spots occur are all in good agreement with energies calculated for coherent scattering from adjacent (100) planes (see Fig. 2). No local minima in width are apparent between these 3-D Bragg energies. Such minima would be expected if oligatomic (<5) step heights predominated [11]. However, it is not certain that local minima in width would be pronounced enough to be observed against the diffuse background level in the present experiment. If a large proportion of multiatomic ($\geq$5) step heights were present, the Lu and Lagally [11] calculations indicate that the spot width would be almost constant except at beam energies very close to the 3-D Bragg conditions, where a sharp spot would be seen. Since the electrochemically cycled Pt (100) surfaces show a more gradual transition between minimum and maximum spot size, it would

appear that multiatomic step heights are not present in great numbers.

The maximum LEED spot size from a randomly stepped surface is inversely related to the mean terrace width. Lu and Lagally [11] have calculated the normalized full width at half maximum intensity versus mean terrace width for a number of step distributions. Although the high diffuse background and present data collection methods complicate the exact determination of this width, it lies at ~0.1 of the Brillouin zone width for the surfaces cycled to 1.58 V. For a geometric (random) distribution of terrace widths with monatomic step heights, this spot width corresponds to a mean terrace width of ~5 atoms or 13 Å. Coulometric repulsions between steps lead one to expect a somewhat more highly correlated terrace width distribution. Henzler [28] obtained the best fit to beam profile data for etched semiconductor surfaces with an emperical distribution of terrace sizes somewhat more highly correlated than a geometric distribution. Assumption of this emperical distribution in the present experiment leads to a mean terrace width of ~7 atoms or 19 Å. The presence of multiatomic step heights would decrease the apparent mean terrace width corresponding to a given spot width. Our results to date indicate the most probably configuration of the 1.58 V cycled surface to be primarily a random up-and-down series of monatomic atomic steps with a mean terrace width of ~5-7 atom spacings, but the quantitative contribution of oligatomic steps remains to be determined. Improved spot profile measurement techniques and a decrease in the diffuse background should allow a more precise description of the surface, including the variation of step density (if any) as a function of the surface crystallographic direction.

The Auger spectrum of the 1.58 V cycled surface separated from the electrolyte at 0.4 V is essentially the same as that shown in Fig. 7d. However, if separation is made while holding at the upper limit of the sweep, a quite different Auger spectrum is observed. An O (510 eV)/Pt (238 eV) Auger ration of ~3 is measured, and no C impurity is seen, probably because of irreversible electrochemical oxidation of the contaminants and a lower sticking coefficient for backfill gas impurities on the oxygen-covered surface. A detailed analysis of the electrosorbed oxygen layer will make up a separate report [29].

(4.2) Cyclic Voltammetry on UHV-Prepared Pt(100) and (111) Surfaces

The first potential sweep of a UHV- prepared Pt(100) surface after contact with electrolyte at 0.48 V RHE is shown in Fig. 9. The hydrogen electrosorption region between 0.02 V and 0.35 V RHE shows an excess of cathodic charge corresponding to 0.6 e^-/Pt. On the anodic sweep above 0.35 V there is a sharp cathodic spike with a charge corresponding to 0.4 e^-/Pt (calculated by subtracting the expected anodic double layer charging curve). This result is similar to previous curves for Pt(100) in aqueous HF obtained by the group of Yeager [6]. An anodic peak of 0.4 e^-/Pt occurs at 0.76 V, and a cathodic peak of ~0.3 e^-/Pt is found at 0.45 V. These features are quite stable to repetitive cycling between the potential limits shown, though the sharpness of the cathodic spike decreases after ~5 cycles. The sum of the excess cathodic charge in the hydrogen region and the cathodic spike yields an uncompensated cathodic charge of nearly 1 e^-/Pt which is stable upon repetitive cycling to 0.8 V. As reported by Yeager, the cathodic spike is seen only after sweeping into or holding within the potential region below 0.2 V. Figure 10 shows the

cathodic spike and then the results of sweeping repetitively between 0.33 and 0.82 V. The anodic and cathodic peaks decay in concert, each cathodic peak representing ~25% less charge than the preceeding anodic peak. This correlated decay suggests that the two peaks are manifestations of the same surface entity. As the sweep rate is decreased from 500 mV/S to 6 mV/S the potential spacing between the anodic and cathodic peaks decreases by at most 0.060 V (~15%), and the charges corresponding to the peaks are essentially unchanged. The peaks are thus due to a surface process which is complex and highly irreversible. Once the couple has decayed during such cycling, it can be regenerated by sweeping into or holding within the hydrogen region, procedures which also regenerate the cathodic spike. Figure 11 shows that the size of the irreversible couple peaks are directly related to that of the cathodic spike, implicating the same surface entity in the origin of all three features.

When UHV- prepared Pt (100) surfaces were contacted with electrolyte without potentiostatic control, a potential of 0.56 V RHE was measured. In an experiment using a counterelectrode in the external reservoir, the single crystal electrode potential jumped from the cathodic spike (0.35 V) to 0.56 V and back again during a momentary loss of potentiostatic control while the compliance voltage of the potentiostat was exceeded. These results suggest that the cathodic spike is due to the reduction of a chemically formed surface species which tends to buffer the electrode at a potential within the irreversible couple. Details of this interpretation will be given in the discussion section.

Repeated cycling well into the oxygen electrosorption region removed the cathodic spike and irreversible couple, yielding voltammograms (Fig. 12) similar to those found in other studies of Pt (100) [1,2,3,4]. Although abrupt changes were seen after a single cycle above 1.2 V, complete suppression of the cathodic spike required ~20 cycles. Voltammograms corresponding to the right-hand LEED patterns of Fig. 8 showed traces of the cathodic spike and couple. Once the unusual features had been suppressed by cycling they could be regenerated neither by holding in the hydrogen electrosorption region nor by draining the electrolyte and reexposing the surface to backfill gases - a repetition of surface preparation in UHV was required to restore the spike.

(4.2.1) Alternate Surface Preparations

The cathodic spike and irreversible couple were also seen after oxygen adsorption or argon sputtering, two vacuum techniques which suppress the 5 x 20 reconstruction of clean surface. Dosing in 10^{-5} torr O_2 with the crystal at 600 K produced a 1 x 1 LEED pattern and left submonolayer quantities of oxygen on the surface. Ar-sputtering without a subsequent annealing step gave a 1 x 1 LEED pattern showing beam energy dependent broadening due to random steps and some beam energy independent broadening due to a decrease in ordered domain size. While electrochemical cycling into the oxygen region suppressed the cathodic spike and couple, argon-sputtering, which produced similar changes in the long-range order of the surface, did not.

The intentional adsorption of carbon monoxide on Pt (100) in UHV accentuated the cathodic spike and couple. Figure 13 shows the first two sweeps of a surface dosed with a 6L (one Langmuir equals 10^{-6} torr sec)

CO exposure. In the work of Barteau. et al. [30], such an exposure yields a saturation coverage of 0.75 monolayer. On the first sweep both cathodic and anodic charge in the hydrogen region are only 0.3 $\underline{e}^-$/Pt due to blocking of hydrogen adsorption sites by CO. A very sharp anodic peak, with an area of 1.5 $\underline{e}^-$/Pt, is seen at 0.76 V RHE. Assuming that CO does saturate at 75% coverage, this charge corresponds to 2.0 $\underline{e}^-$/CO. After sweep reversal two cathodic peaks at 0.58 and 0.48 V with a combined area of 1.1 $\underline{e}^-$/Pt appear, followed by cathodic and anodic charges of 1.1 $\underline{e}^-$/Pt and 0.7 $\underline{e}^-$/Pt, respectively, in the hydrogen region. At 0.9 $\underline{e}^-$/Pt, the cathodic spike is larger than any on surfaces not intentionally dosed with CO, and the following, slightly split, anodic peak corresponds to 0.8 $\underline{e}^-$/Pt. Subsequent sweeps show little decay in the cathodic spike, and the couple appears as single anodic and cathodic peaks at 0.76 V and 0.40 V, respectively. Thus after several cycles the CO- dosed surface yields voltammograms qualitatively similar to those from nominally clean Pt (100), but with a quantitatively enhanced cathodic spike and couple. The implications of the CO results will be considered in the discussion section.

(4.2.2) Cyclic Voltammetry on Pt (111).

The voltammetry of UHV- prepared Pt (111), as shown in Fig. 14, is free of any cathodic spike but shows other unusual features similar to those reported for flame- cleaned Pt (111) beads in $HClO_4$ by Clavilier [5]. As on Pt (100), an anodic peak occurs at 0.76 V. However, on Pt (111) this peak is reversible and has a shoulder at 0.67 V. The sharp anodic peak at 1.06 V, also reported by Clavilier, has no analog on the (100) surface. Upon cycling to higher potentials this peak disappears and the lowest potential peak in the hydrogen region grows to give a

voltammogram (Fig. 15) closer to those reported in most previous studies of Pt (111) [1,2,4].

(5) DISCUSSION

(5.1) Electrochemical cycling and surface reconstruction

LEED results indicate that cycling well into the oxygen electrosorption region introduces random steps into the Pt (100) surface, while cycling just to the edge of the oxygen region does not. The restructuring process is shown schematically in Fig. 16. During the excursion into the oxygen region, Pt atoms move up out of (and O atoms or hydroxyl groups move down into) the surface as a thin (O/Pt surface atomic ratio ≈1) oxide layer is formed. Upon reduction of the surface, Pt atoms move laterally and/or vertically into 3-D lattice sites but do not restore the initial smooth surface. The majority of surface sites retain the symmetry of the (100)-1 x 1 surface, but new step sites with the nearest neighbor symmetries found on (111) and (110) planes are introduced. Future detailed measurements of the LEED beam angular profiles as functions of surface azimuthal direction and beam energy should identify the relative density of steps in different symmetry directions and allow more precise determinations of both step height distributions and mean terrace widths. Studies of how changing the anodic limit of the potential sweep affects surface restructuring may identify the onset potential for place exchange [31] and help clarify the mechanisms of Pt oxidation. LEED may enable the identification of techniques for electrochemical surface cleaning leading to minimal surface structuring, thereby improving the precision of single-crystal electrode studies done without benefit of coupled ultra-high vacuum equipment.

(5.2) Cyclic voltammetry on UHV-prepared Pt (100) and (111)

The strikingly different voltammetric behavior of Pt (100) and (111) surfaces on the first sweeps after immersion is indicative of an unusually strong structure dependence of the reactions occurring at these surfaces. However, the identification of just what reactions are occurring is uncertain. We consider in the following discussion two distinctly different interpretations of the behavior observed: (1) the behavior represents the interaction of clean, ordered Pt surfaces with HF solution; (2) the behavior represents the superposition of the clean Pt-H_2O-HF system and complex interaction of ordered Pt surfaces with impurity species. Both will be considered here, though our data seems somewhat more consistent with the second interpretation.

The sharpness of the cathodic spike seen on Pt (100) tempts one to identify it with the well-known 1 x 1 → 5 x 20 surface phase transition. Although Rutherford backscattering has shown that more than one monolayer's worth of Pt atoms move when this transition is induced by hydrogen adsorption [32], the difference in the number of surface Pt atoms in the hexagonally and square-packed planes amounts to a decrease of only 15% of a monolayer, with the excess atoms moving either onto the surface as random adatoms or into the bulk. Based on this 15%, the charge in the cathodic spike per Pt atom moved out of the packed plane is 2.7 $\underline{e}^-$ for the "clean" surface and 6 $\underline{e}^-$ for the CO-saturated surface. This charge seems too great to be explained as hydrogen adsorption onto adatoms or onto additional atoms in the plane (1 x 1 → 5 x 20) or through the reorientation of electrolyte dipoles in the double layer due to the surface phase transformation. The persistence of the cathodic spike on the argon-sputtered and oxygen-dosed surfaces,

which had the 1 x 1 structure even *in vacuo* further suggest that the cathodic spike is not due to the surface phase transformation, but rather to a more complex chemical process which occurs only upon sites with the nearest-neighbor symmetry of the Pt (100) - 1 x 1 surface.

Because of the complexity of the voltammetric behavior observed on the Pt (100) surface, it is helpful to depict the behavior in a schematic sequence of possible reactions. It should be emphasized that the scheme shown is schematic and not literal, in that neither the electroactive species nor the stoichiometry represented are necessarily known. The sequence which describes what is observed on the (100) surface on cycling between 0.02 - 0.8V is as follows:

Pt-Red + H^+ + $\underline{e}^-$	$\xrightarrow{\text{Pt-H}}$	Pt-Red-H	hydrogenation step	$Q_c > Q_a$
Pt-Red - H + H_2O	$\xrightarrow{\text{Pt-}}$	Pt-Ox + H_2	chemical step	
Pt-Ox + $\underline{e}^-$	$\longrightarrow$	Pt-Red	cathodic spike	
Pt-Red	$\longrightarrow$	Pt-Ox + $\underline{e}^-$	anodic peak	redox couple
Pt-Ox + e^-	$\longrightarrow$	Pt-Red	cathodic peak	

Step (1) involves the hydrogenation (in the presence of adsorbed hydrogen) of an adsorbed species. Step (2) is the chemical disproportionation of the product of the preceeding step into gaseous hydrogen and an oxidized product which buffered the electrode potential at 0.58 eV in several experiments (see section 3). This step is catalyzed by free Pt sites (or possibly by hydronium ions) and is triggered by the normal electrooxidation of adsorbed hydrogen. The hydrogen evolution accounts

for the excess of cathodic charge. When the surface is under potentiostatic control the adsorbed product of step (2) is reduced, resulting in the cathodic spike. Re-oxidation, this time electrochemically, occurs in step (4), followed by reduction in step (5). The identity of the species Red and Ox is not known, but it seems unlikely that the electroactive species are just those in the Pt-H_2O-HF system. The enhancement of of the effects by the intentional adsorption of CO, a common vacuum system background gas, and the reaction of Red with adsorbed hydrogen suggest that Red·H may be related to the "reduced CO_2" of Giner [33]. However, CO may enhance the cathodic spike and couple by simply blocking the adsorption of other, less easily oxidized impurities; and a clean-surface explanation cannot be excluded on this basis alone. Sweeping the surface above 1.2 V RHE, a technique which irreversibly oxidizes many surface impurities, suppressed the cathodic spike and redox couple. When the long-range structural modification induced by potential cycling were simulated by argon-sputtering the surface before contact with electrolyte, the spike and couple were still observed. Thus our present observations on Pt (100) seem more consistent with the chemistry of a ubiquitous (to stainless steel systems at least) surface impurity than with that of a clean surface.

It is not a simple matter to relate the very different character of the voltammetric behavior of the Pt (111) surface to that of the Pt (100) surface. Clavilier [5] has assigned the sharp, reversible peaks at ca. 0.8 V to a very strongly bound (ca. $-\Delta H_{ads} \simeq 40$ kcal/mol) state of hydrogen unique to the ordered (111) surface. The only evidence cited in

support of this assignment was the kinetic reversibility. While we have no new direct observations to refute this assignment, such a strongly adsorbed state of hydrogen is not consistent with what is known about the Pt H_{ads} bond at the vacuum interface. It is known that hydrogen is adsorbed on highly ordered Pt (111) surfaces with a zero-coverage heat of adsorbtion of 11 kcal/mol and the dipole moment for Pt H_{ads} has the negative end at Pt [34]. Hydrogen is also more strongly bound at the ordered (100) surface [35], or at step-like imperfections in the low-index surfaces [36]. For hydrogen to be bound at ca. 40 kcal/mol on Pt (111) in solution requires invoking an argument that the electrical double layer enhances the bond energy. But the direction of the electric field gradient in the most prevalent theory of the double-layer [37] is of opposite polarity to the dipole moment of Pt H_{ads}, which would tend to decrease not increase the Pt H_{ads} bond energy (relative to the vacuum value). On the other hand, we acknowledge that it is difficult to make an assignment of this peak at ca. 0.8 V to other electroactive species because of the kinetic reversibility. It is thermodynamically possible that this peak corresponds to a water dissociation process, such as the formation of surface - OH species [31]. Vacuum studies of oxygen and water on Pt (111) surfaces [38] suggest that surface - OH formation is kinetically facile, so it seems at least feasible that the sharp peak at ca. 0.8 V could be a reversible - OH species. However, potential cycling to 1.4 - 1.6 V removed this peak without causing loss of the short-range (5-7 atoms) order in the surface, suggesting that the peak is associated with an electroactive species that is irreversibly oxidized at high potential. In this report the peaks seen in voltammetry curves for Pt (100) and (111) at 0.5 - 1.0 V are

similar, i.e. they disappear upon cycling to higher potentials. It is tempting to equate these peaks to the same species on both surfaces with a dramatic difference in reversibility due to structure sensitivity, but the assignment must in reality await more definitive evidence than has been produced to date.

ACKNOWLEDGMENT

This work was supported by the Assistant Secretary for Conservation and Renewable Energy, Office of Advanced Conservation Technology, Division of Electrochemical Systems Resources of the U.S. Department of Energy under Contract Number DE-AC03-76SF00098.

REFERENCES

1.) F. G. Will, J. Electrochem. Soc., 112 (1965) 451.

2.) A. Hubbard, R. Ishikawa and J. Kutakaru, J. Electroanal. Chem., 86 (1978) 271.

3.) K. Yamamoto, D. Kolb, R. Koetz and G. Lempfuhl, J. Electroanal. Chem., 96 (1979) 233.

4.) P. N. Ross, Jr., Surf. Sci., 102 (1981) 463.

5.) J. Clavilier, J. Electroanal. Chem., 107 (1980) 211.

6.) E. Yeager, J. Electrochem. Soc., 128 (1981) 160C.

7.) C. J. Davisson and L. H. Germer, Phys. Rev., 30 (1927) 705.

8.) W. P. Ellis and R. L. Schwoebel, Surf. Sci., 11 (1968) 82.

9.) M. Henzler, Surf. Sci., 19 (1970) 159.

10.) J. E. Houston and R. L. Park, Surf. Sci., 26 (1971) 269.

11.) T. M. Lu and M. G. Lagally, Surf. Sci., to be published; T. M. Lu, S. R. Anderson, M. G. Lagally and G. C. Wang, J. Vac. Sci. Technol., 17 (1980) 207.

12.) J. E. Houston and R. L. Park, Surf. Sci., 21 (1970) 209.

13.) M. Henzler in H. Ibach (Ed.), Electron Spectroscopy for Surface Analysis, Topics in Current Physics, Vol. 4, Springer, Berlin, 1977, p. 117.

14.) M. G. Lagally in R. Vanselow and R. Howe (Ed.), Chemistry and Physics of Solid Surfaces IV, Springer Series in Chemical Physics, Vol. 20, Springer, Berlin, 1982, p. 281.

15.) M. Henzler, to be published.

16.) J. A. Martin and M. G. Lagally, to be published.

17.) F. Jona, Surf. Sci., 8 (1967) 57.

18.) J. G. Gordon, II, Extended Abstracts, 82-1 (1982), The Electrochemical Society, Pennington, NJ, p. 1055.

19.) M. A. Van Hove, R. J. Koestner, P. C. Stair, J. P. Biberian, L. L. Kesmodel, I. Bartos and G. A. Somorjai, Surf. Sci., 103 (1981) 189.

20.) J. L. Gland and G. A. Somorjai, Advan. Colloid Interface Sci., 5 (1976) 205.

21.) S. M. Davis, B. E. Gordon, M. Press and G. A. Somorjai, J. Vac. Sci. Technol., 19 (1981) 231.

22.) S. M. Davis, Ph.D Thesis, University of California, Berkeley, 1981.

23.) G. A. Garwood and A. T. Hubbard, Surf. Sci., 112 (1981) 281.

24.) M. Salmeron and G. A. Somorjai, J. Phys. Chem., 86 (1982) 341.

25.) T. E. Fischer and S. R. Keleman, Surf. Sci., 69 (1977) 485.

26.) B. Lang, P. Legare and G. Maire, Surf. Sci., 46 (1975) 89.

27.) J. C. Tracy and P. W. Palmberg, J. Chem. Phys., 51 (1969) 4852.

28.) M. Henzler, Surf. Sci., 73 (1978) 240.

29.) F. T. Wagner and P. N. Ross, Jr., to be published.

30.) M. A. Barteau, E. I. Ko and R. J. Madix, Surf. Sci., 102 (1981) 99.

31.) H. Angerstein-Kozlowska, B. E. Conway and W. B. A. Sharp, J. Electroanal. Chem., 43 (1973) 9.

32.) P. R. Norton, J. A. Davies, D. K. Creber, C. W. Sitter and T. E. Jackman, Surf. Sci., 108 (1981) 205.

33.) J. Giner, Electrochim. Acta, 8 (1963) 857 and 9, (1964) 63.

34.) K. Christmann, G. Ertl and T. Pignet, Surf. Sci., 54, (1976) 365.

35.) R. McCabe and L. Schmidt, in Proc. 7th Int. Vac. Congr. and 3rd Int. Conf. on Solid Surf. (Vienna, 1977), p. 1201.

36.) K. Christmann and G. Ertl, Surf. Sci., 60 (1976) 365.

37.) J. Bockris, M. Devanathan and K. Muller, Proc. Roy. Soc. London, A297 (1963).

38.) G. Fisher and J. Gland, Surf. Sci., 94 (1980) 446.

FIGURES

Fig. 1. Ewald construction for LEED. After Ref. 14.

Fig. 2. Ewald constructions for surfaces with Pt (100) terraces and monatomic steps running along the a.) [010] and b.) [011] directions. Intersections of the Ewald sphere with filled small circles indicate sharp single LEED beams. Open small circles indicate split LEED beams for periodic steps or broadened beams for random steps. By scaling beam energies to the nearest neighbor distance, this figure can be applied to any fcc (100) surface.

Fig. 3. Ewald construction for a surface with monatomic step height and random terrace widths. After Ref. 14.

Fig. 4. UHV-electrochemical apparatus: a.) surface analysis chamber, b.) transfer chamber, c.) magnetically coupled manipulators, d.) external electrolyte reservoir, e.) gate valves, f.) manipulator for Pt wire probe electrode.

Fig. 5. LEED pattern for clean Pt (100)-5 x 20 surface.

Fig. 6. LEED pattern for Pt (100) a.) after Ar backfill, b.) after contact with electrolyte and ten cycles to 0.82 V.

Fig. 7. Auger spectra for Pt (100): in descending order a.) clean, b.) after transfer without backfill, c.) after Ar backfill, d.) after contact with electrolyte and separation at 0.4 V. E_p = 3 kV, V_m = 2 V_{p-p}.

Fig. 8. LEED patterns for Pt (100) after ten cycles to 0.82 V (left) or 1.58 V (right). Incident energy: a.) 178 eV, b.) 134 eV, c.) 114 eV.

Fig. 9. First-sweep cyclic voltammogram for UHV-prepared Pt (100) contacted at 0.48 V with 0.3 M HF. Sweep rate 100 mV/s. Contact area 0.4 cm^2.

Fig. 10. Voltammogram for Pt (100) held 30 sec. at 0.08 V, then swept at 100 mV/s to higher potentials and cycled 0.33-0.82 V. Contact area 0.4 cm^2.

Fig. 11. Voltammograms for Pt (100) held for thirty seconds at (in decending order) a.) 0.28 V, b.) 0.18 V, c.) 0.08 V, then cycled at 100 mV/s above 0.33 V. Contact area 0.2 cm^2.

Fig. 12. 20th sweep to 1.58 V at 100 mV/s for Pt (100) in 0.3 MHF. Contact area 0.25 cm^2.

Fig. 13. First and second sweeps at 100 mV/s for Pt (100) dosed in UHV with 6 L CO. Contact at 0.48 V, contact area 0.25 cm^2.

Fig. 14. Voltammograms for Pt (111) in 0.3 MHF swept at 100 mV/s to progressively higher potentials. Contact area 0.2 cm^2.

Fig. 15. Voltammogram for Pt (111) after having been cycled to 1.33 V. Contact area ~0.7 cm^2, 100 mV/s.

Fig. 16. Cross-sectional schematic of Pt (100) surface: a.) before cycling, b.) oxidized, at upper limit of potential sweep, c.) after electrochemical reduction of b.

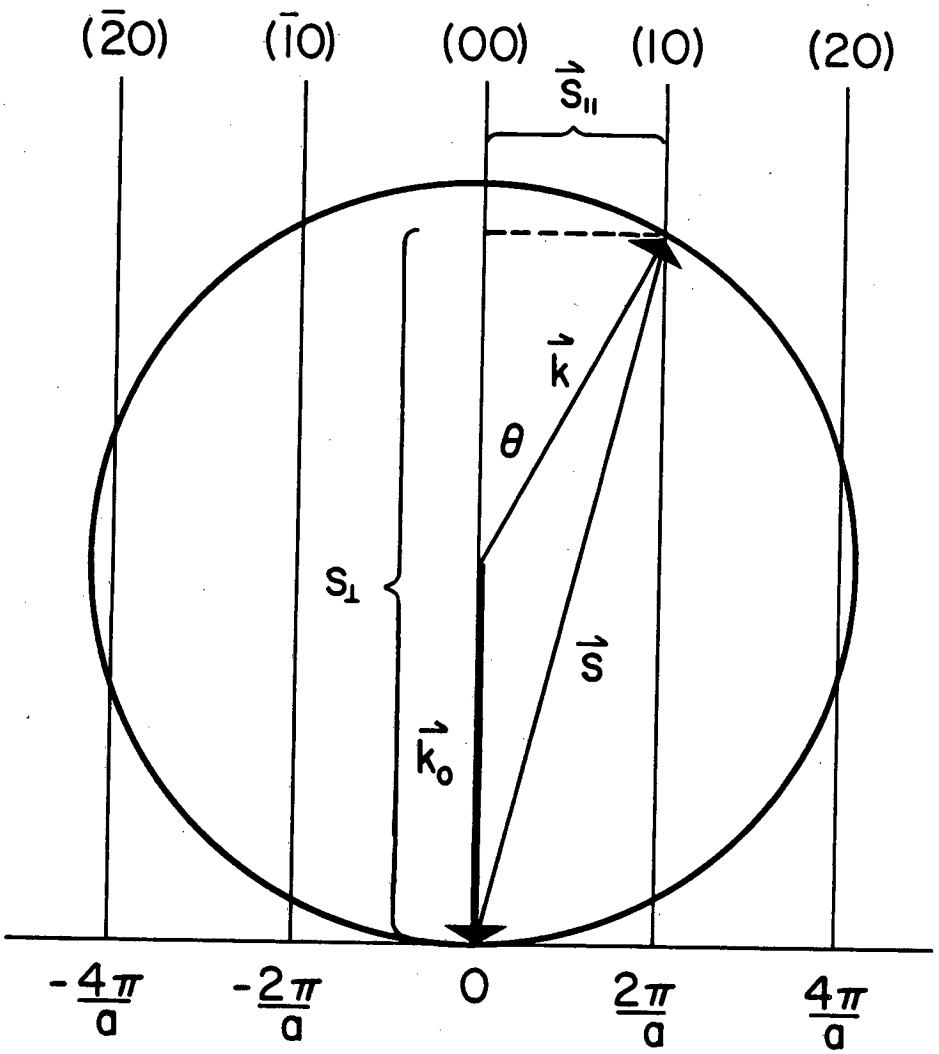

XBL 827 – 882

Fig. 1

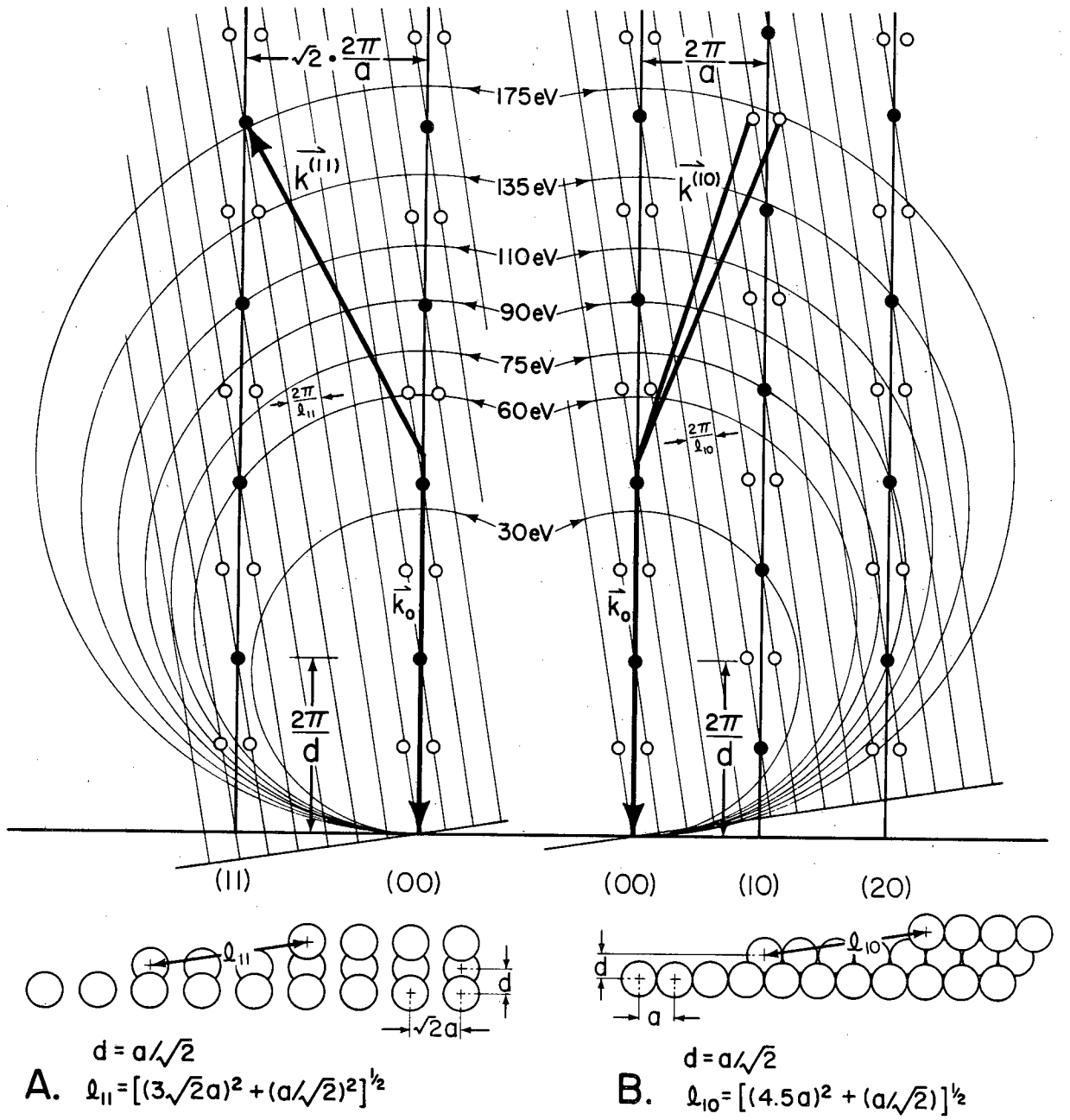

$d = a/\sqrt{2}$

A. $\ell_{11} = [(3\sqrt{2}a)^2 + (a/\sqrt{2})^2]^{1/2}$

$d = a/\sqrt{2}$

B. $\ell_{10} = [(4.5a)^2 + (a/\sqrt{2})]^{1/2}$

XBL 827-926

Fig. 2
a & b

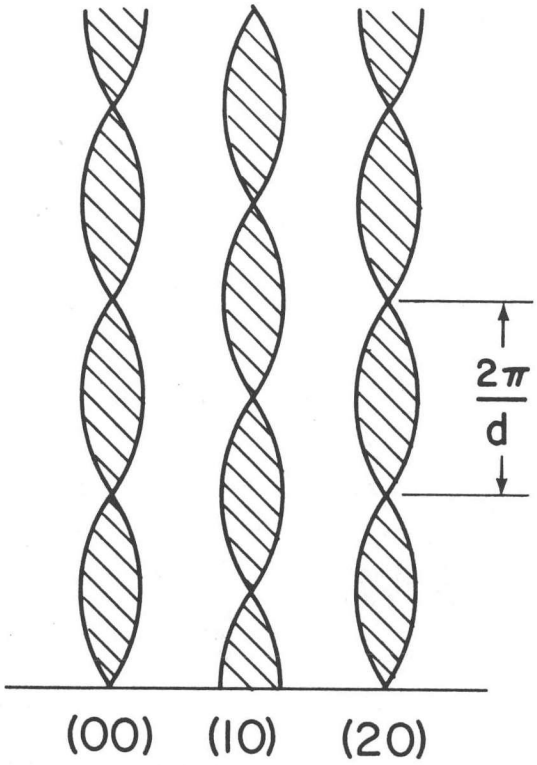

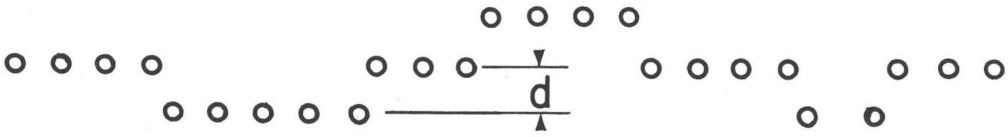

XBL 827 – 881

Fig. 3

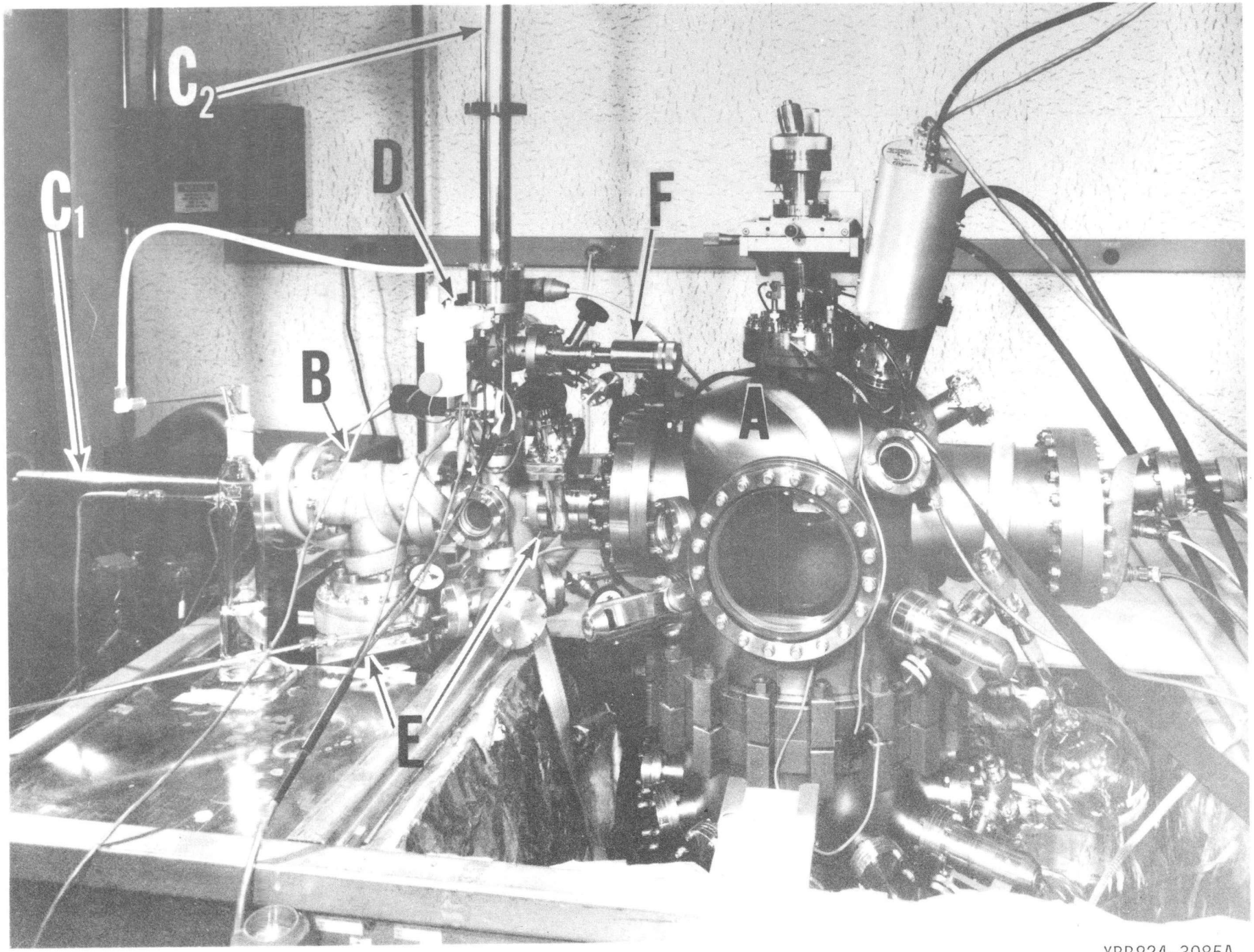

XBB824-3085A

Fig. 4

Pt (100) 5x20

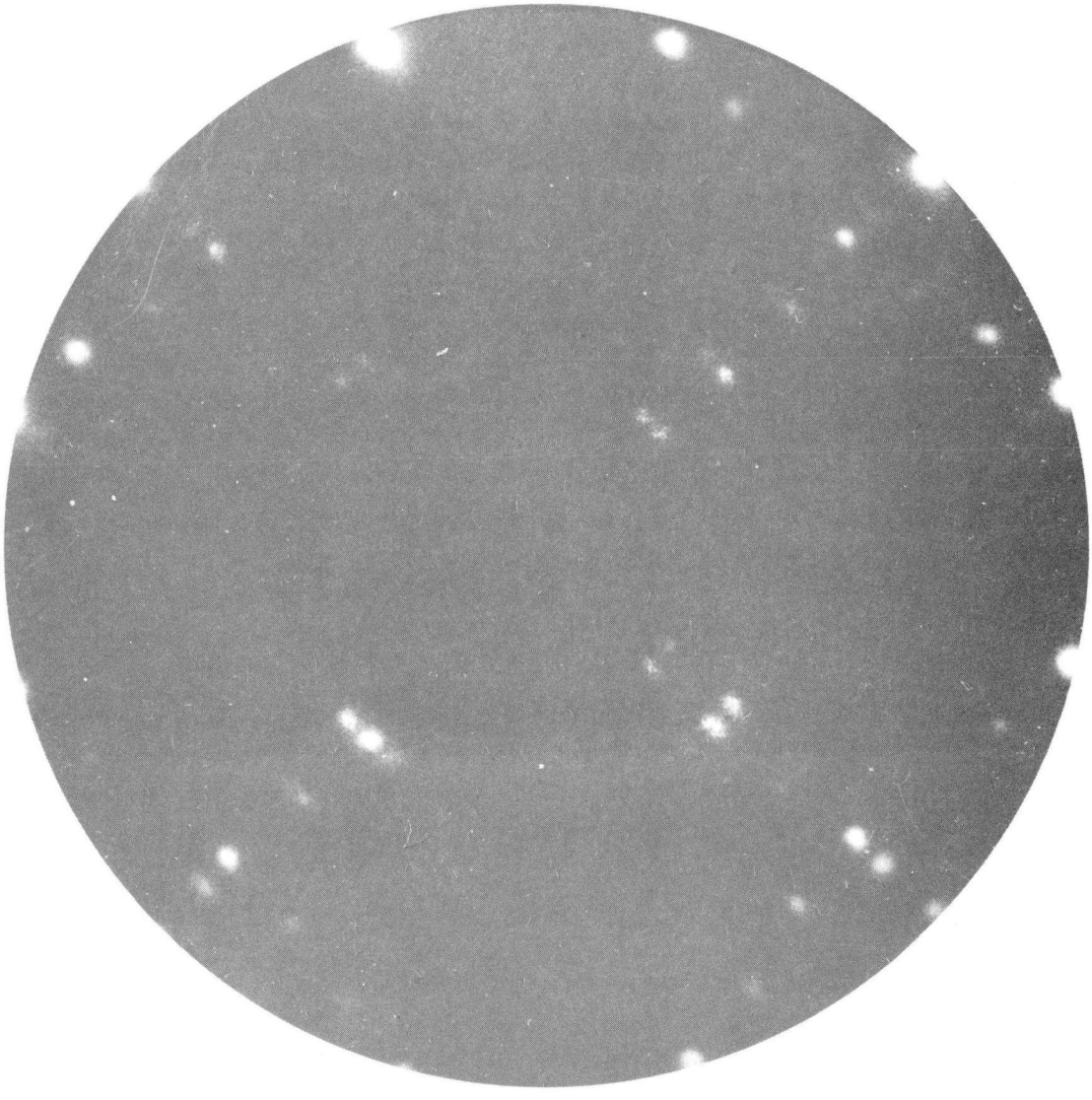

42 eV

XBB827-6080

Fig. 5

LEED after backfill

134 eV

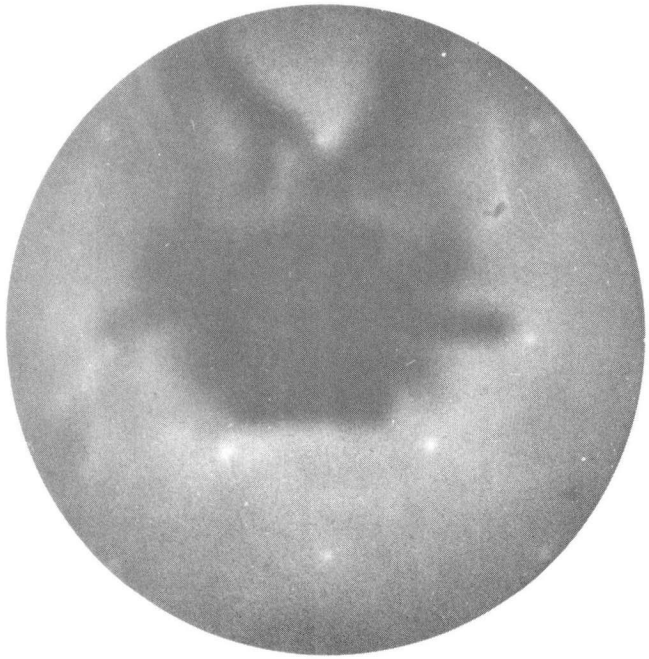

no contact
with electrolyte

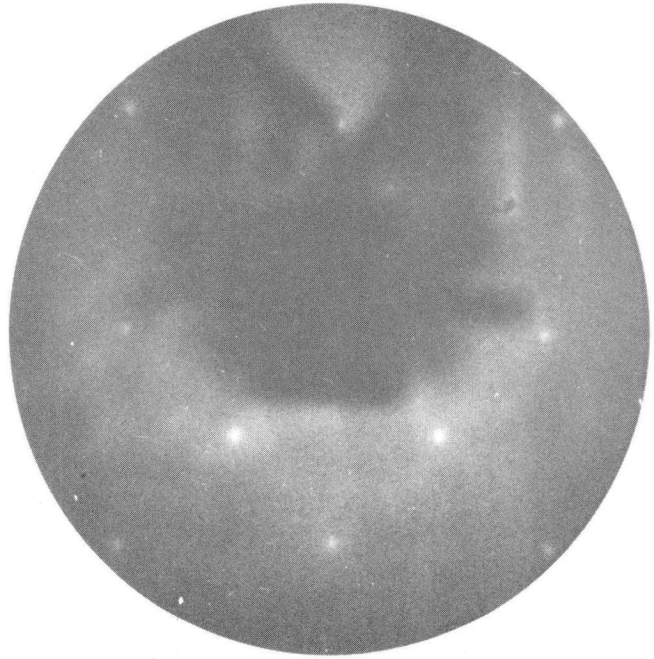

after ten cycles
to 0·82 V (RHE)

XBB824-4022A

Fig. 6
a & b

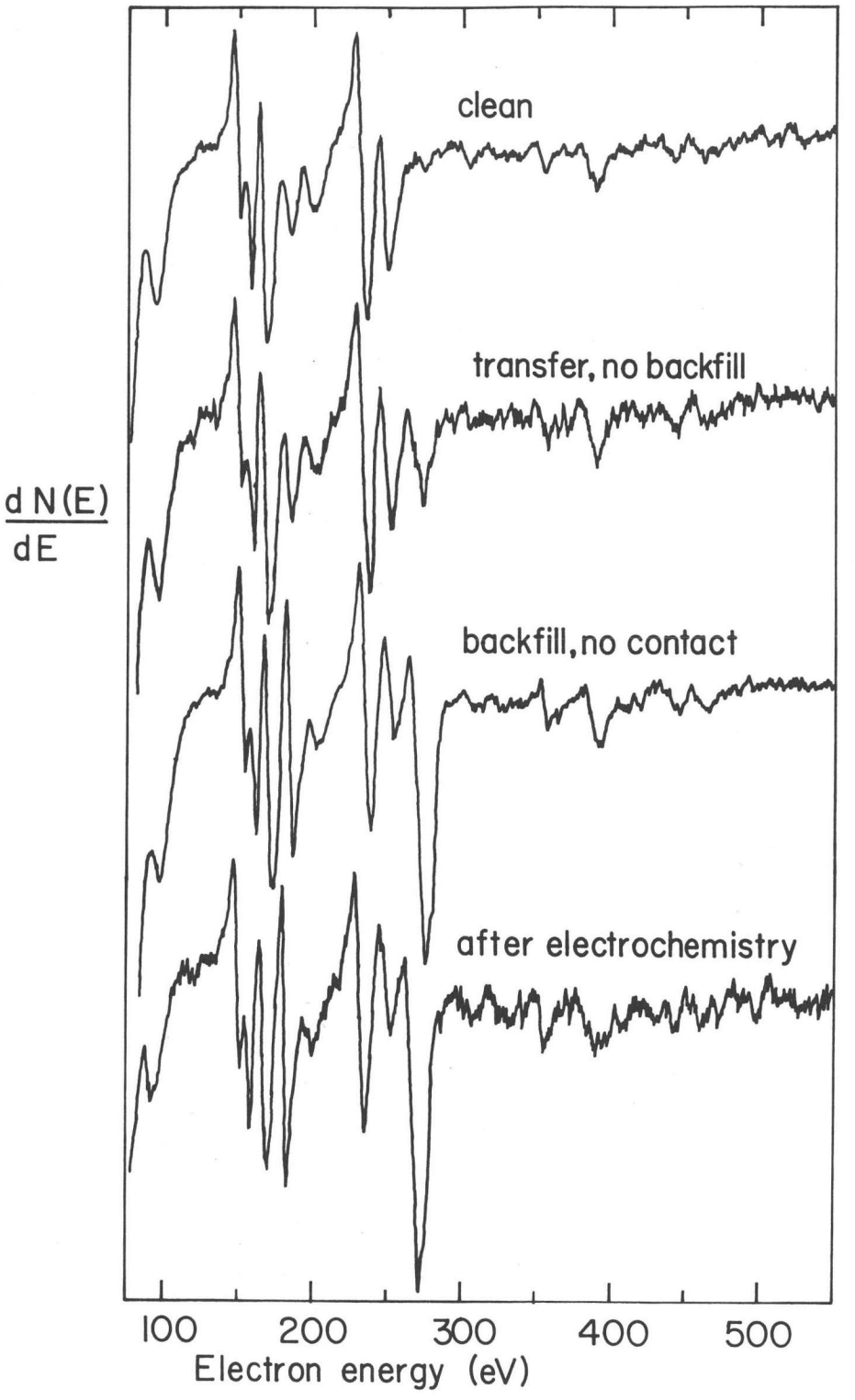

XBL 825-9764

Fig. 7
a,b,c & d

LEED 178 eV
after ten cycles

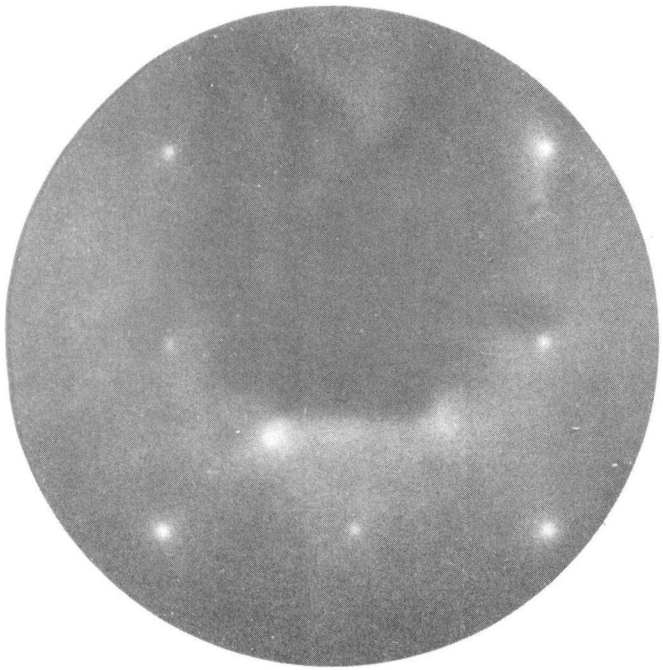

to 0·82 V (RHE)

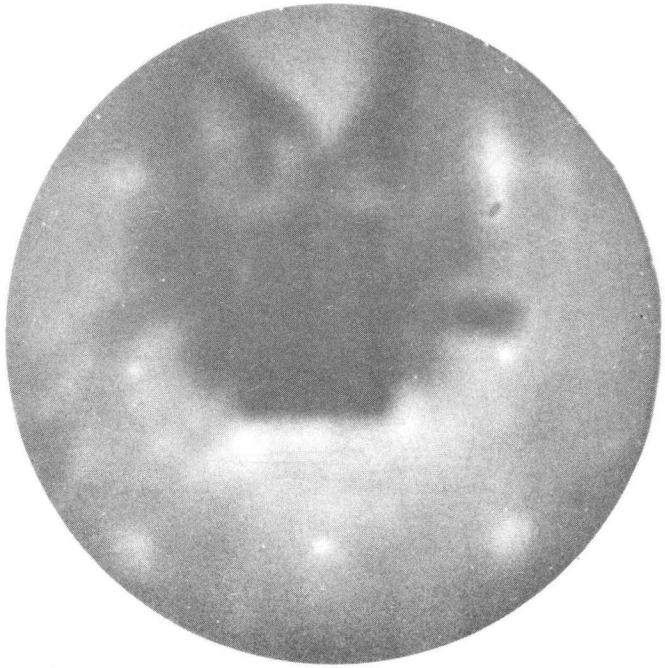

to 1·58 V (RHE)

XBB824-4023

Fig. 8a

LEED 134 eV

after ten cycles

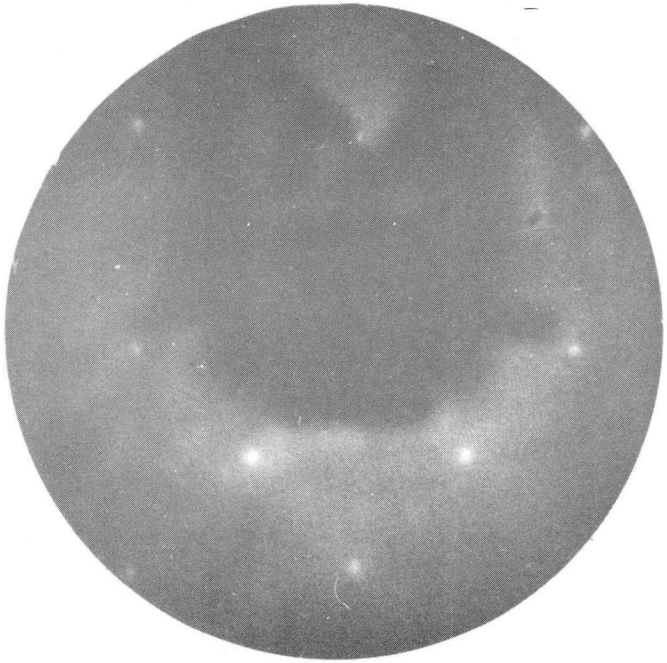

to 0·82 V (RHE)

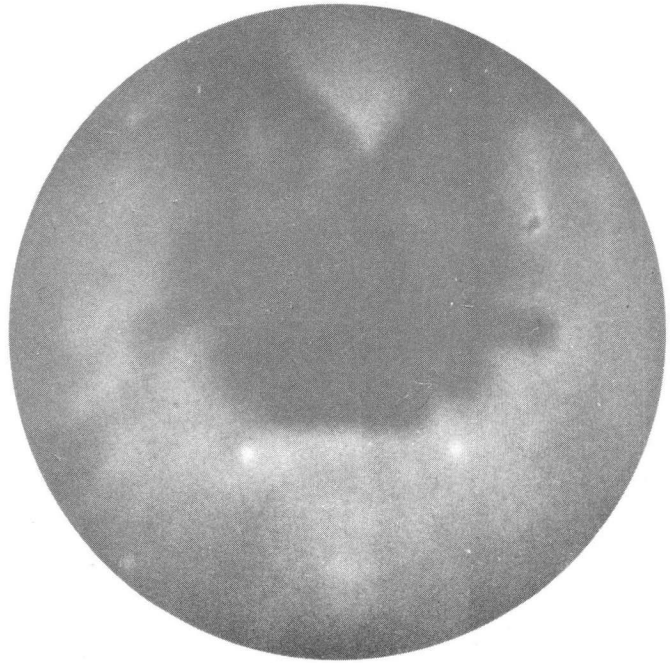

to 1·58 V (RHE)

XBB824-4022

Fig. 8b

LEED 114 eV

after ten cycles

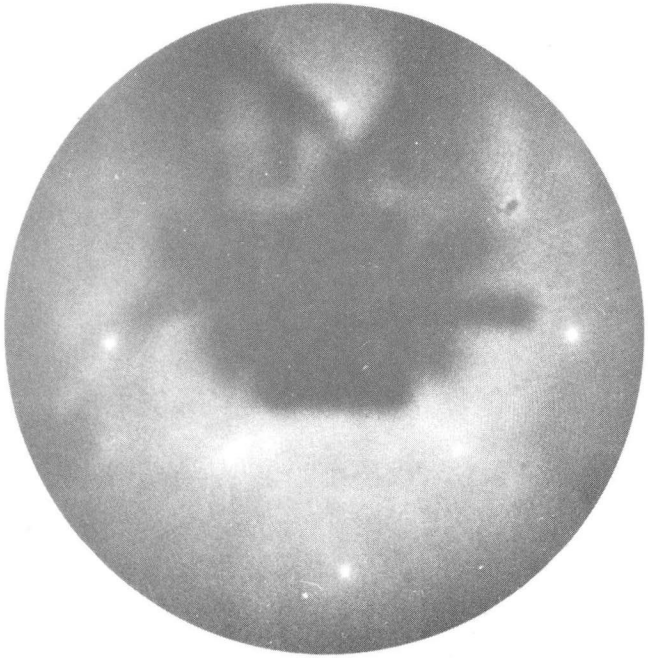

to 0·82 V (RHE)

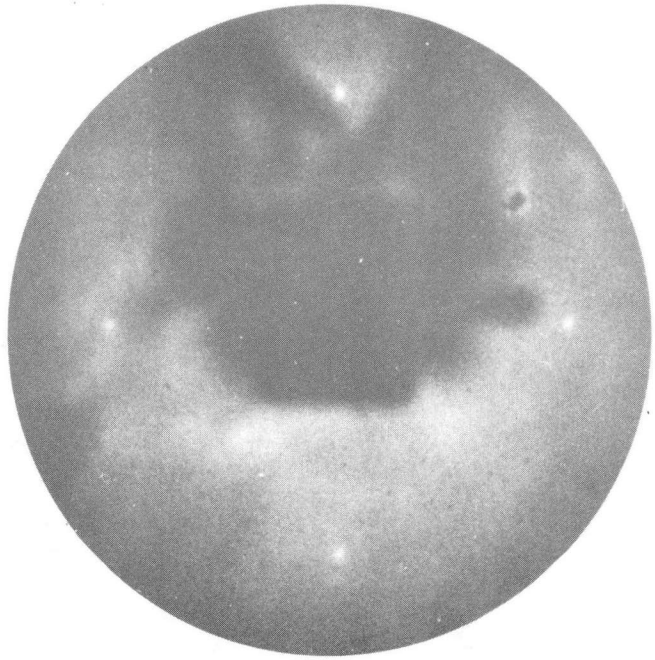

to 1·58 V (RHE)

XBB824-4021

Fig. 8c

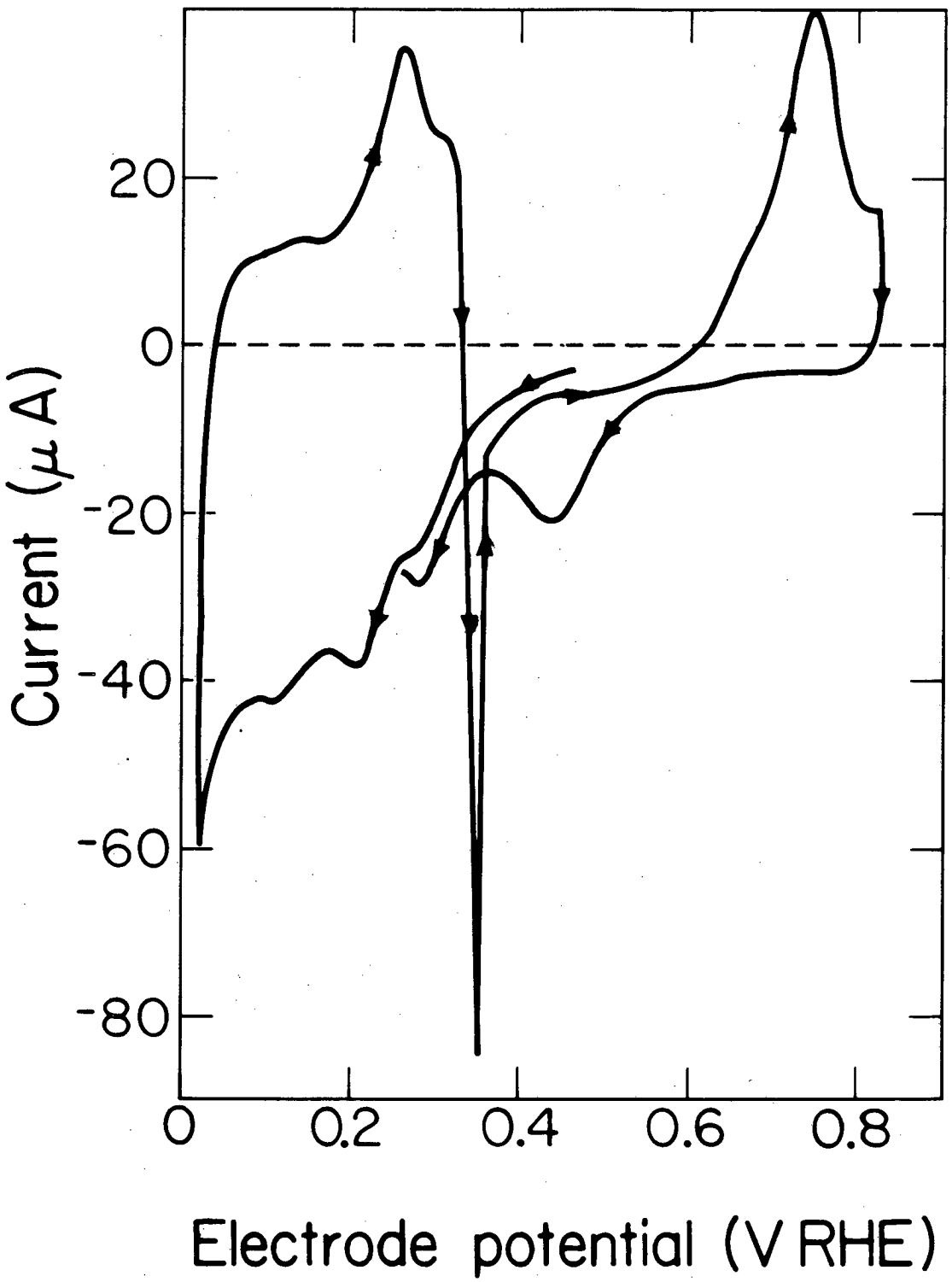

XBL 824-446

Fig. 9

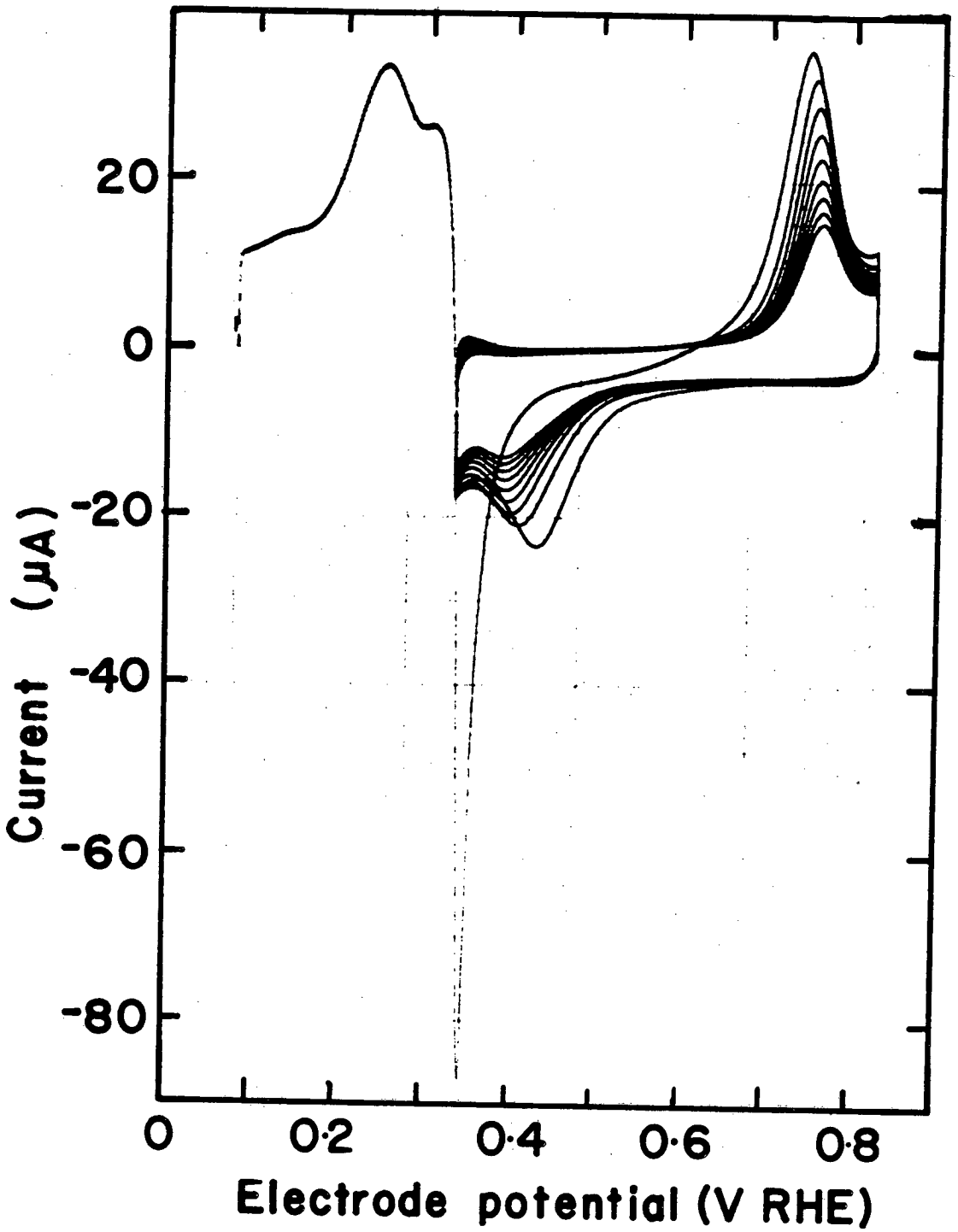

XBL 824-9362

Fig. 10

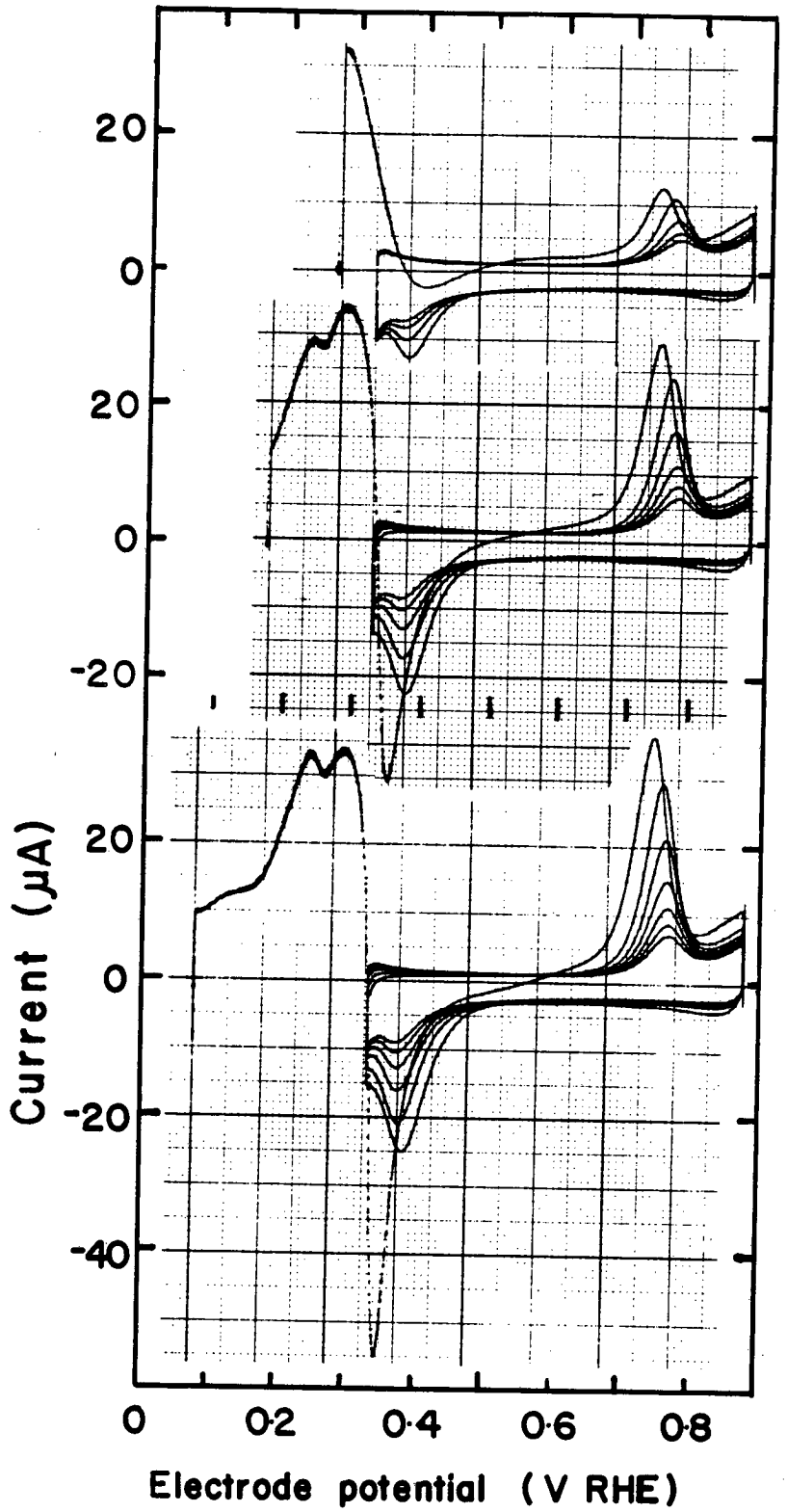

XBL 824-9365

Fig. 11
a,b,c

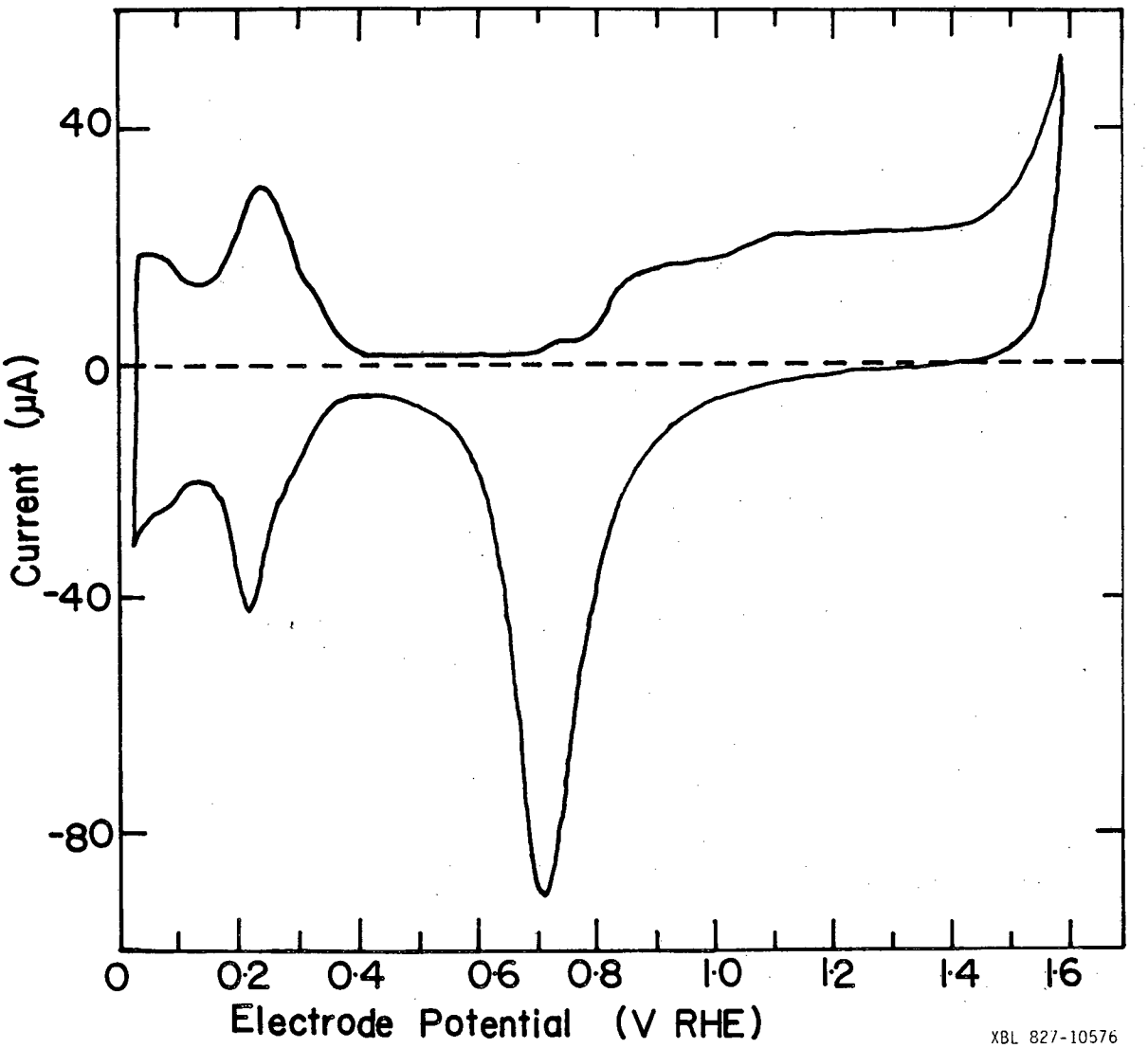
40
0
-40
-80
Current (μA)
0
0·2
0·4
0·6
0·8
1·0
1·2
1·4
1·6
Electrode Potential (V RHE)
XBL 827-10576

Fig. 12

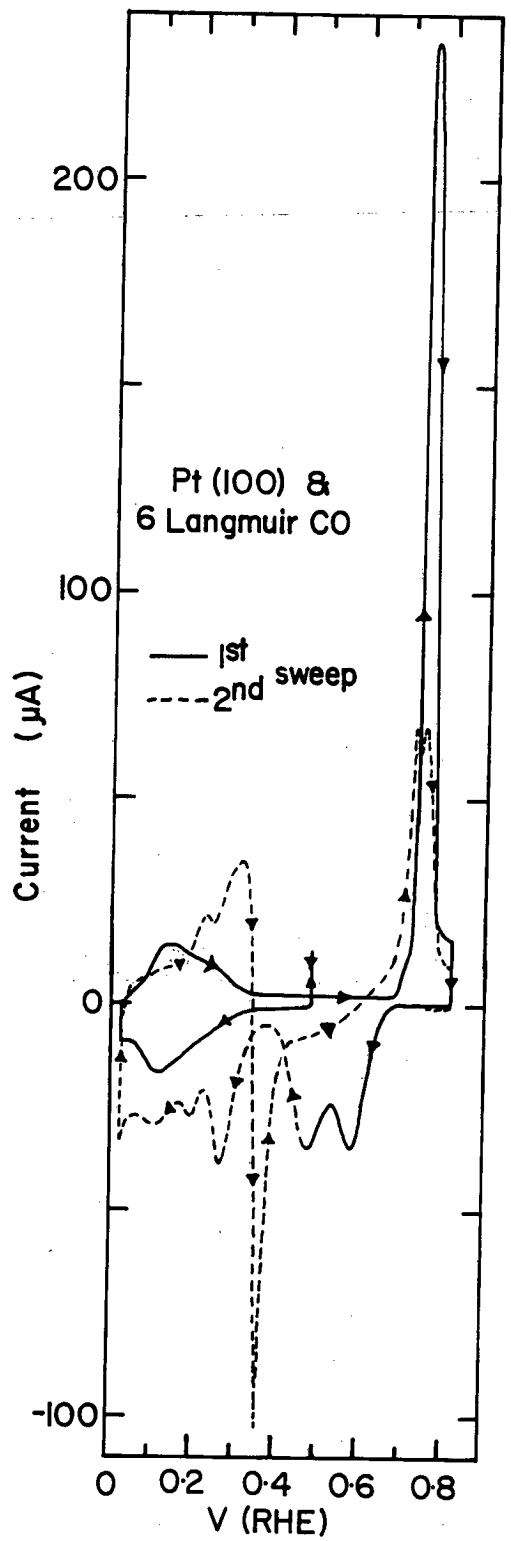

XBL 825-9879

Fig. 13

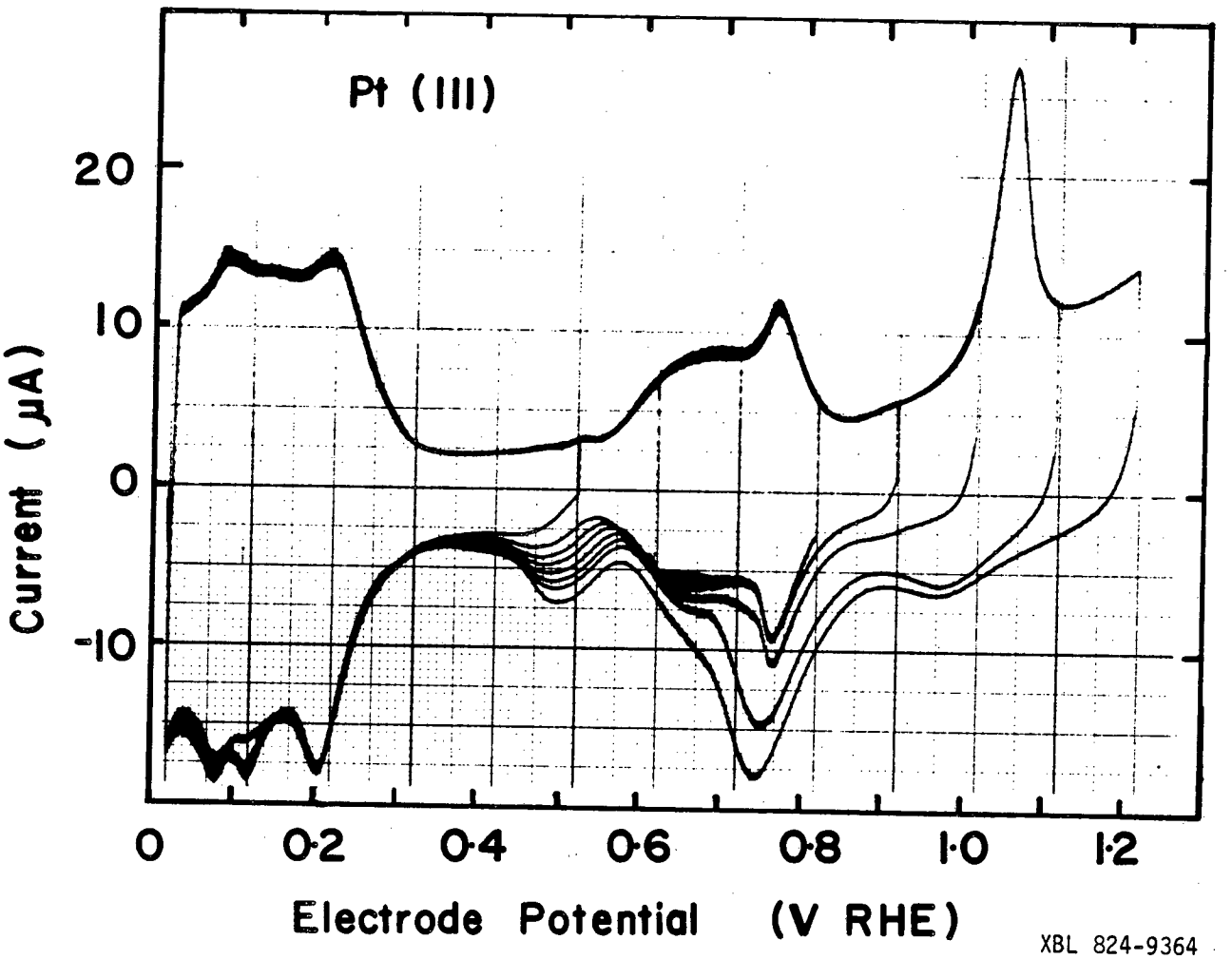
Pt (111)
20
10
0
-10
Current (μA)
0
0·2
0·4
0·6
0·8
1·0
1·2
Electrode Potential (V RHE)
XBL 824-9364

Fig. 14

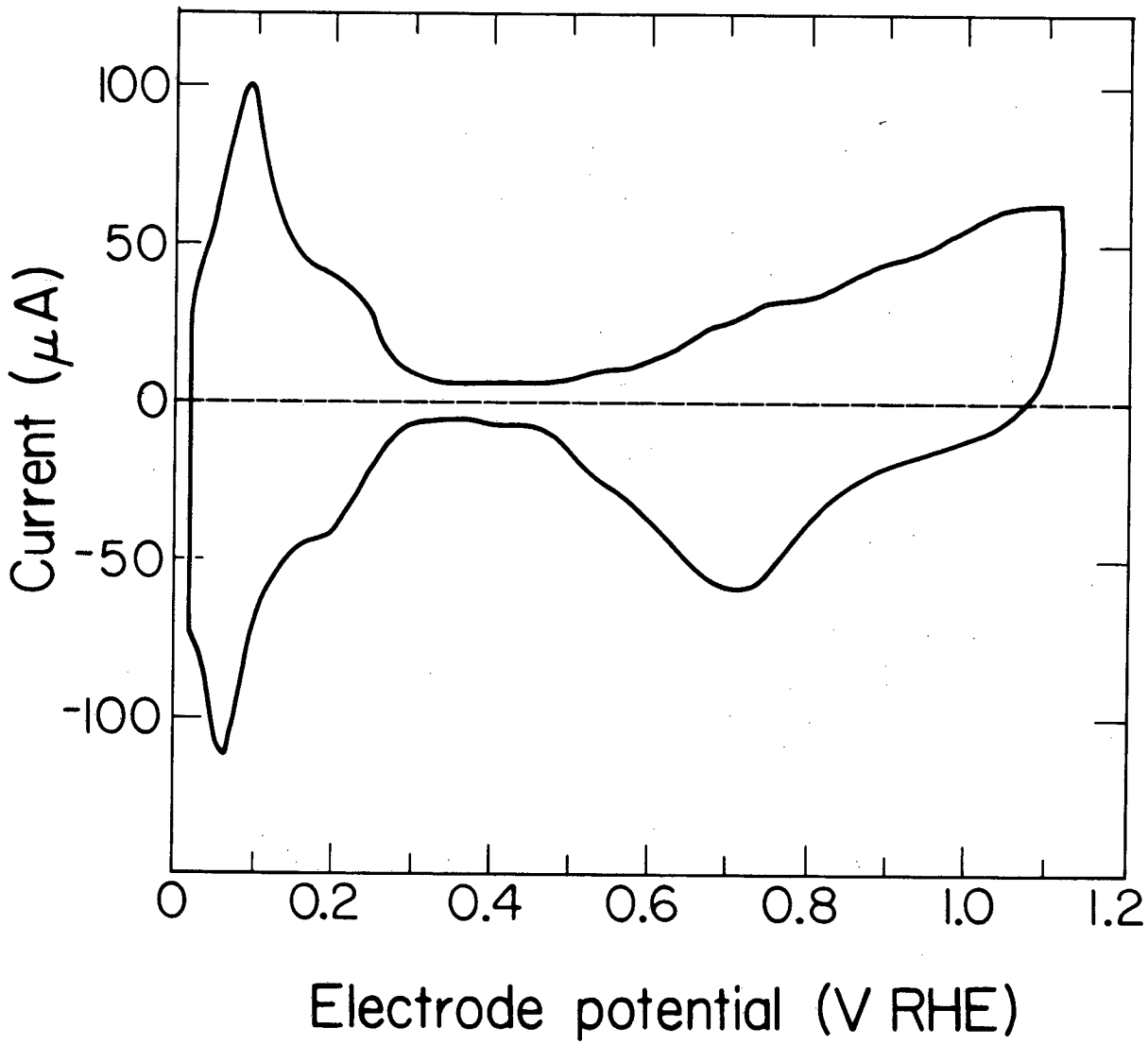

XBL 824-444

Fig. 15

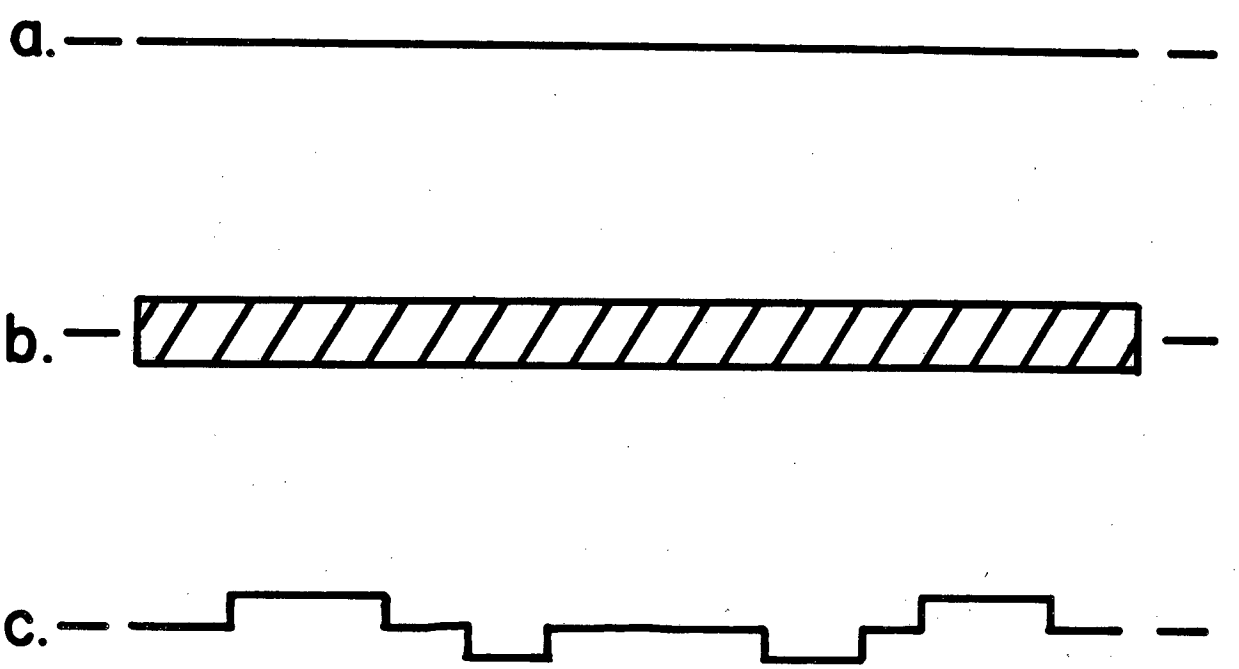

XBL 827-10722

Fig. 16

This report was done with support from the Department of Energy. Any conclusions or opinions expressed in this report represent solely those of the author(s) and not necessarily those of The Regents of the University of California, the Lawrence Berkeley Laboratory or the Department of Energy.

Reference to a company or product name does not imply approval or recommendation of the product by the University of California or the U.S. Department of Energy to the exclusion of others that may be suitable.

TECHNICAL INFORMATION DEPARTMENT
LAWRENCE BERKELEY LABORATORY
UNIVERSITY OF CALIFORNIA
BERKELEY, CALIFORNIA 94720